Perimenopause promotes neuroinflammation in select hippocampal regions in a mouse model of Alzheimer's disease

Roberta Marongiu[1,3,4]†, Jimcy Platholi[1,2]†, Laibak Park[1], Fangmin Yu[1], Garrett Sommer[1], Clara Woods[1], Teresa A. Milner[1]††* and Michael J. Glass[1]††

1. Feil Family Brain and Mind Research Institute, Weill Cornell Medicine, 407 East 61st St, New York, NY 10065 USA
2. Anesthesiology Department, Weill Cornell Medicine, 1300 York Ave, New York, NY 10065 USA
3. Neurological Surgery Department, Weill Cornell Medicine, 1300 York Ave, New York, NY 10065 USA
4. Genetic Medicine Department, Weill Cornell Medicine, 1300 York Ave, New York, NY 10065.

†These authors contributed equally to this work and share first authorship.
††These authors contributed equally to this work and share senior authorship.

*Corresponding author for manuscript:
Dr. Teresa A. Milner
Feil Family Brain and Mind Research Institute
Weill Cornell Medicine
407 East 61st Street, RM 307
New York, NY 10065 USA
Phone: (646) 962-8274
Email: tmilner@med.cornell.edu

Corresponding authors, communications: Teresa A. Milner - tmilner@med.cornell.edu
Michael J. Glass - mjg2003@med.cornell.edu

Number of pages (excluding abstract, figure legends, acknowledgements, and references): 17
Number of figures: 8
Number of Supplementary figures: 2
Number of Tables: 0

Abbreviated title: 5XFAD mice, behavior & hippocampal glia

Submission for 2025 Special Issue: "Estrogens and Neurodegeneration: a Link Between Menopause and Alzheimer's Diseases in Women" hosted by Frontiers in Molecular Biosciences

Conflict of interest: The authors declare no competing financial interests.

Keywords: amyloid beta, astrocyte, microglia, ovarian failure, pyramidal cell

ABBREVIATIONS

Aβ, beta amyloid
AD, Alzheimer's disease
AOF, accelerated ovarian failure
cCA1, caudal CA1
Cen, central hilus
cDG, caudal DG
DG, dentate gyrus
GFAP, glial fibrillary acidic protein
Iba1, ionized calcium binding adapter molecule 1
IFG, infragranular blade
PB, phosphate buffer
PCL, pyramidal cell layer
rCA1, rostral CA1
rDG, rostral DG
SG, supragranular blade
SLM, stratum lacunosum-moleculare
SLu, stratum lucidum
SO, stratum oriens
SR, stratum radiatum
TS, Tris saline
VCD, 4-vinylcyclohexene diepoxide

ABSTRACT

Alzheimer's disease (AD) is the most common neurodegenerative disorder characterized by age-dependent amyloid beta (Aβ) aggregation and accumulation, neuroinflammation, and cognitive deficits. Significantly, there are prominent sex differences in the risk, onset, progression, and severity of AD, as well as response to therapies, with disease burden disproportionately affecting women. Although menopause onset (i.e., perimenopause) may be a critical transition stage for AD susceptibility in women, the role of early ovarian decline in initial disease pathology, particularly key neuroinflammatory processes, is not well understood. To study this, we developed a unique mouse model of perimenopausal AD by combining an accelerated ovarian failure (AOF) model of menopause induced by 4-vinylcyclohexene diepoxide (VCD) with the 5xFAD transgenic AD mouse model. To target early stages of disease progression, 5xFAD females were studied at a young age (~4 months) and at the beginning stage of ovarian failure analogous to human perimenopause (termed "peri-AOF"), and compared to age-matched males. Assessment of neuropathology was performed by immunohistochemical labeling of Aβ as well as markers of astrocyte and microglia activity in the hippocampus, a brain region involved in learning and memory that is deleteriously impacted during AD. Our results show that genotype, AOF, and sex contributed to AD-like pathology. Aggregation of Aβ was heightened in female 5xFAD mice and further increased at peri-AOF, with hippocampal subregion specificity. Further, select increases in glial activation also paralleled Aβ pathology in distinct hippocampal subregions. However, cognitive function was not affected by peri-AOF. These findings align with the hypothesis that perimenopause constitutes a period of susceptibility for AD pathogenesis in women.

INTRODUCTION

Dementia is a leading contributor to the global burden of disease [1] with Alzheimer's disease (AD) constituting approximately 50-70% of cases [2]. AD is characterized by progressive neurodegeneration and cognitive dysfunction [3, 4]. A main hallmark of AD neuropathology is the accumulation of parenchymal plaques containing aggregated amyloid-beta (Aβ) in the cerebral cortex and the hippocampal formation [5]. In addition to Aβ deposition, AD involves a complex set of related neurodegenerative processes including neuroinflammation [6]. In AD animal models, neuroinflammation characterized by the activation of reactive astrocytes and microglia [7] is one of the earliest pathological manifestations, likely contributing to synaptic and neuronal loss.

Important sex differences in AD are well documented, with women experiencing a disproportionately greater disease burden [8]. The incidence of AD is at least two-fold higher in women compared to men [2] with women exhibiting faster disease progression [9] and greater cognitive impairment at comparable stages of AD [10]. Perimenopause, the transitional phase of irregular gonadal hormonal production and cycling before full menopause, may be a particularly vulnerable period for the onset of mild cognitive impairment and AD. This is supported by evidence that low endogenous estrogen levels are associated with increased AD risk [11], and that early or late age at menopause is associated with an elevated or decreased risk for AD, respectively [12-14]. Furthermore, there is growing evidence that initiating estrogen replacement soon after menopause may help mitigate dementia development [15]. Significantly, perimenopause is also associated with declines in brain volume [16] and increases in Aβ expression [16, 17]. Despite these associations, the mechanisms underlying the heightened perimenopausal risk for AD, particularly those related to neuroinflammation and cognitive decline in the hippocampus, remain unclear.

Animal models may help elucidate the mechanisms driving perimenopausal AD risk. The commonly used 5xFAD transgenic mouse model, which expresses five familial mutations in two AD risk genes, exhibits increased Aβ production and plaque formation that parallels AD pathology [18]. Notably, sex differences have been reported in 5xFAD mice, with females showing earlier increases in inflammatory gene expression [19], glial markers [20, 21] as well as Aβ levels [19, 20, 22]. This neuropathology correlates with worse cognitive performance, in some studies [19-21], but not all [23, 24]. Markers of brain inflammation appear as early as three months of age, suggesting that sex differences in AD-like pathology emerge at a prodromal stage [19]. Additionally, female 5xFAD mice show increased hippocampal Aβ and elevated expression of

immune-related genes and proteins compared to age-matched males [18, 25-29]. These sex differences may be linked to changes in estrogen signaling [30-32]. Thus, combining mouse models of AD with perimenopause in females may help to isolate the effects of hormonal changes on AD neuropathology.

The 4-vinylcyclohexene diepoxide (VCD) ovatoxin mimics perimenopause in rodents by producing accelerated ovarian failure (AOF) paralleling the irregular hormone fluctuations seen during human perimenopause (termed "peri-AOF" in rodents) before transitioning to full menopause [33-35]. This model allows for controlled induction of AOF at various times/ages following sexual maturity in younger animals, reducing the confounding effects of chronological aging, a main AD risk factor [33-35]. The VCD model has been used to investigate how ovarian failure influences metabolic [36-38], aging [39], and cerebrovascular [40] factors to influence cognitive function, brain plasticity and amyloid pathology in wild-type (WT) mice or in mouse models of cognitive impairment and dementia. However, the impact of early ovarian failure (peri-AOF) on Aβ-related pathology and neuroinflammatory response in 5xFAD mice is unknown.

We investigated whether peri-AOF contributes to hippocampal neuroinflammation in young 5xFAD mice treated with VCD. A granular assessment of Aβ levels and glial markers of neuroinflammation was conducted by analyzing all major hippocampal subfields at rostral and caudal levels. Cognitive performance was assessed using tests of learning and memory. To characterize early AD-like neuropathology, we focused on young (~4 months) 5xFAD mice. Age-matched male mice were also tested to evaluate the effect of biological sex.

EXPERIMENTAL PROCEDURES

ANIMALS. Young adult (~2 month-old at the initiation of the experiments [41]) C57BL/6 WT mice (n= 22 females and n= 11males) and transgenic 5xFAD (C57BL/6 background; n= 22 female and n= 11 male) mice were bred and maintained in a colony at Weill Cornell Medicine (WCM). Breeding pairs of hemizygous 5xFAD mice were obtained from the Jackson Laboratory (Bar Harbor, ME; JAX MMRRC stock#034840). Mice were bred in-house and genotyped prior to experimentation. 5xFAD mice express human APP and PSEN1 transgenes with a total of five AD-linked mutations under the control of the Thy1 promoter. This mouse model exhibits early-onset parenchymal Aβ aggregation correlated with cognitive deficits [42, 43]. Amyloid deposition begins in the cerebral parenchyma at 2-3 months of age, with little accumulation in the cerebral vasculature, and amyloid plaques are found throughout the hippocampus and cortex by six months [18, 44] . Astrogliosis and microgliosis begin around two months, developing in parallel

with plaque deposition [18]. Mice were housed in groups of three to four animals per cage and maintained on a 12-hr light/dark cycle (lights out 18:00 hours) with *ad libitum* access to water and rodent chow. At euthanasia, mice weighed 23-32 grams. All experiments were approved by the WCM Institutional Animal Care and Use Committees and followed the National Institutes of Health guidelines for the Care and Use of Laboratory Animals guidelines.

AOF model of perimenopause. AOF induction by VCD treatment in mice has been shown to recapitulate the gradual hormonal fluctuations that correspond to peri- and post-menopause in humans (reviewed in [45, 46]). The AOF model can be used to separate hormonal effects from aging effects and can be applied to any mouse genotype [33-35]. Low dose VCD injections selectively deplete ovarian primary follicles without negatively affecting peripheral tissues, kidney, or liver function [34, 47-49]. VCD does not directly increase inflammation markers in the brain, including the hippocampus [33].

AOF induction. Gonadally intact 53-58-postnatal-day-old female mice received 130 mg/kg VCD (cat. # S453005 Millipore Sigma, St. Louis, MO) in sesame oil (cat. # 8008-74-0 Millipore Sigma) for 5 days per week for 3 weeks [35, 45]. Control mice received injections of sesame oil only. Prior studies from our lab and others [33, 47, 50] established the peri-AOF stage as occurring 58 days after the first VCD injection. At this stage (~3.5 months old), the mice exhibit irregular, prolonged estrous cycles and elevated plasma follicle stimulating hormone [50-52]. Behavioral assessments of VCD- and oil-treated females, as well as aged-matched males, were initiated when mice were about 4 months of age (the peri-AOF stage of VCD mice). A timeline of the experimental procedures is shown in Figure 1.

Estrous cycle assessment. At euthanasia, vaginal smears [53] were collected to determine the terminal estrous cycle stage via cytological examination. Estrous cycle phases were classified as proestrus (high estrogen), estrus (declining estrogen), or diestrus (low estrogen and progesterone). Most females were in estrus or diestrus at euthanasia.

***ANTIBODIES*. 4G8:** A mouse monoclonal antibody raised against amino acid residues 17-24 of beta-amyloid (4G8, Biolegend Cat. # 800701) was employed. This antibody recognizes abnormally processed isoforms as well as precursor APP forms (manufacturer's instructions), and labels both parenchymal and vascular Aβ aggregates [54-57]. **GFAP:** A rabbit polyclonal antibody (Abcam # ab7260; lot # GR20948-21; RRID:AB_305808) raised against full-length human GFAP was used. On Western blot, this antibody recognized 48 kDa and 55 kDa GFAP bands

128 (manufacturer's datasheet). **Iba1:** A rabbit polyclonal antibody raised against a synthetic peptide
129 corresponding to the C-terminus of Iba1 (#SAR6502; 019-19741 FUJIFILM Wako Pure Chemical
130 Corporation) was employed. The antibody reacts with rat, mouse and human Iba1 and recognizes
131 a 17 kDa band protein on Western blot (manufacturer's datasheet). These antibodies have been
132 used in our prior studies [58, 59].
133
134 ***BRAIN FIXATION AND HISTOLOGY.*** Mouse brains were processed for immunocytochemistry
135 using established procedures in our labs [60]. Briefly, mice were deeply anesthetized with sodium
136 pentobarbital (150 mg/kg, i.p.), and then perfused with saline. The brains were extracted, bisected
137 sagittally, and the right hemisphere fixed in 4% paraformaldehyde in 0.1M phosphate buffer (PB,
138 pH 7.4) for 24 hrs on a shaker (70 rpm) at 4°C. The forebrain containing the hippocampus was
139 sectioned (40 µm thick) on a vibratome (VT1000X Leica Microsystems, Buffalo Grove, IL) and
140 stored in cryoprotectant (30% sucrose, 30% ethylene glycol in PB) at -20°C until
141 immunocytochemical processing.
142 For each experiment, one rostral (-2.00 to -2.70 mm from Bregma [61]) or caudal (-2.90
143 to -3.50 mm from Bregma [61]) hippocampal section per animal was selected and then punch
144 coded in the cortex. Tissue sections from each experimental group were pooled into single
145 containers to ensure identical reagent exposure [60].
146
147 ***LIGHT MICROSCOPIC IMMUNOCYTOCHEMISTRY***. Hippocampal sections from each
148 genotype/sex group were processed for 4G8, Iba1 or GFAP (n= 11/group). Sections were rinsed
149 in 0.1M Tris-saline (TS; pH 7.6), blocked with 0.5% bovine serum albumin (BSA) in TS for 30 min,
150 and incubated in primary antibodies mouse anti-4G8 (1:4000), rabbit anti-GFAP (1:6000) or rabbit
151 anti-Iba-1 (1:4000) diluted in 0.1% Triton-X and 0.1% BSA in TS for 24-hrs at room temperature
152 followed by 24-hrs at +4°C. Next, sections were rinsed in TS and incubated in either biotin-
153 conjugated goat anti-rabbit IgG (for GFAP and Iba1; #111-065-144, Jackson ImmunoResearch
154 Inc., West Grove, PA; RRID:AB_2337965) or goat anti-mouse IgG (for 4G8; # 115-065-166,
155 Jackson ImmunoResearch Inc.; RRID:AB_2338569) in 0.1% BSA and TS. Sections were washed
156 in TS and incubated in Avidin Biotin Complex (ABC; Vectastain Elite kit, Vector Laboratories,
157 Burlingame, CA) at half the manufacturer's recommended dilution for 30-min. After rinsing in TS,
158 the bound peroxidase was visualized by reaction in 3,3'-diaminobenzidine (Sigma-Aldrich, St.
159 Louis, MO) and 0.003% hydrogen peroxide in TS for 6-minutes (4G8), 3-min (GFAP), or 8-min
160 (Iba1). All primary and secondary antibody incubations were carried out at 145 rpm, whereas
161 rinses were at 90 rpm on a rotator shaker. Sections were mounted in 0.05 M PB onto gelatin-

162 coated glass slides, dehydrated through an ascending series of alcohol to xylene, and
163 coverslipped with DPX (Sigma-Aldrich).
164
165 ***IMAGE ACQUISITION AND FIELD DENSITOMETRY.*** Quantification for 4G8, Iba1 and GFAP
166 labeling in the hippocampus were performed using previously established densitometric methods
167 [62-64]. To ensure unbiased data quantification, the analysis was performed by investigators
168 blinded to experimental conditions. Images were acquired using a Nikon Eclipse 80i microscope
169 with a Micropublisher 5.0 digital camera (Q-imaging, BC, Canada) and IP Lab software
170 (Scanalytics IPLab, RRID: SCR_002775). ImageJ64 software (Image J, RRID:SCR_003070) was
171 used to measure the pixel density within regions of interest (ROI) in defined hippocampal
172 subregions. ROIs within four subregions of the rostral and caudal hippocampus were selected: 1)
173 **CA1**: stratum oriens (SO), pyramidal cell layer (PCL), stratum radiatum (SR) and stratum
174 lacunosum-moleculare (SLM); 2) **CA2/3a**: SO, PCL, near and distal SR; 3) **CA3b**: SO, PCL,
175 stratum lucidum (SLu) and SR; 4) **Dentate gyrus** (**DG)**: the supragranular blade (SG), the
176 infragranular blade (IFG) and the central hilus (Cen) and 5) **Subiculum** (caudal section).
177 Background pixel density from non-labeled regions (e.g., corpus callosum) was subtracted to
178 control for illumination variability and background labeling. Prior studies [62] demonstrated a
179 strong correlation between pixel density and actual transmittance, confirming measurement
180 accuracy.
181
182 ***BEHAVIORAL ASSESSMENTS***. Mice were tested sequentially over two weeks in the Novel
183 Object Recognition, Y maze, and Barnes maze tasks, as described in prior studies [65, 66]. The
184 same investigator conducted all behavioral tests. Testing occurred at the same time each day,
185 with results recorded using ANY-maze (Stoelting Co.). Mice were habituated to the testing room
186 for 2 hours daily for five days before testing. On testing days, mice were acclimated to the room
187 for 1-hour before each session. The order of the Y-maze and Novel Object tests were
188 counterbalanced, with 24-hour rest between the tests. Behavioral apparatuses were cleaned with
189 70% ethanol between trials.
190
191 **Y-maze**. This test was used to assess spatial working memory as previously described [60]. Mice
192 were placed in a three-arm maze (40 cm long, 9.5 cm high, 4 cm wide) diverging at a 120° from
193 the central point, and allowed to explore two arms for 5 min (training). After 30 min, the previously
194 blocked arm was opened, serving as the novel arm (test trial). The sequence of arm entries
195 (spontaneous alternation) and locomotor activity were recorded for 5 minutes. A Spontaneous

196 alternation was defined as entities into all the 3 arms on consecutive occasions, and was manually
197 recorded from the recorded videos. The total number of arms entered during the sessions, which
198 reflect locomotor activity, also was recorded. The maximum alternation was subsequently
199 calculated by measuring the total number of arm entries minus 2 and the percentage of alternation
200 was calculated as ((actual alternation/maximum alternation)×100).
201
202 **Novel Object Recognition (NOR).** The NOR apparatus (height 30cm x width 28cm x length
203 46cm) consisted of an open field chamber with dim illumination throughout, and it is used to
204 measure spatial and working memory. On day 1 (habituation phase), each mouse was allowed
205 to explore the empty arena for 5-min. On day 2 (familiarization phase), two identical objects (type
206 A) were placed on the floor of the area and the mouse was allowed to explore for 5-min followed
207 by a 30-min rest. For the exploration phase, One of the type A objects was replaced with a novel
208 object (type B) and the mouse was allowed to explore for 5-minutes the familiar and novel objects
209 at the same time. For each phase, the total distance traveled, the average speed, the total object
210 exploration time, and the time spent exploring each one of the two objects was recorded. A
211 discrimination index for day 2 exploration phase was calculated as percentage time spent
212 exploring the novel object out of the total object exploratory time.
213
214 **Barnes maze**. The apparatus consisted of a maze with a 10cm cylindrical white start chamber
215 in the middle, multiple hole and one escape hole in the periphery. Mice were trained in the
216 apparatus for four sequential days. Each training day consisted of 4 trials (with 15 min inter-trial
217 intervals) in the following sequence: 1) Adaption period. The mouse was placed in the white start
218 chamber, and a buzzer was switched on for 10-sec. Following, the mouse was guided to an
219 escape hole for 15-20-sec. The buzzer was turned off and the mouse was allowed to stay in the
220 escape box for 2-min. 2) Spatial acquisition period. The mouse was placed in the start chamber
221 and the buzzer was switched on for 10 seconds. After 10 seconds, the start chamber was
222 removed, and the mouse was allowed to move around the maze to find an escape hole (maximum
223 3-minutes). Immediately after the mouse entered the escape hole, the buzzer was turned off and
224 the mouse was allowed to stay in the tunnel for 1-minute. The average values collected from the
225 spatial acquisition period of all 4 trials in a given training day is used as datapoint in the figures
226 (Fig 8A-D). Twenty-four hours after the last training session, mice underwent the probe trial. For
227 this, the mouse was placed in the maze in the white chamber and the buzzer was switched on.
228 After 10-seconds, the chamber was removed, and the mouse behavior was recorded for 90-

229 seconds. For each mouse, the latency time, errors, total length traveled to find the escape hole
230 were recorded.
231
232 ***IMAGE ADJUSTMENTS FOR FIGURES***. Images were adjusted first for contrast and sharpness
233 in Adobe Photoshop 9.0 (Adobe Photoshop, RRID:SCR_014199). Next, images were imported
234 into Microsoft PowerPoint, where final adjustments to brightness, sharpness and contrast were
235 achieved. Images of different groups in the same figure were similarly adjusted to same
236 brightness and contrast. Adjustments were made to the entire image, none of which significantly
237 altered the appearance of the initial raw image.
238
239 ***DATA ANALYSIS***. Data are presented as means ± SEM. Statistical analyses were conducted
240 using Prism 9 software (Graphpad Prism, RRID:SCR_002798) and significance was set at alpha
241 < 0.05. Group comparisons were performed using analysis of variance (ANOVA; one-, two-,
242 three-way) with Tukey or Sidak's post-hoc tests. Two-group comparisons used Student's t-tests.
243 Specific analysis conducted are indicated in figure legends. Graphs were generated in Prism 9
244 software.
245
246 **RESULTS**
247 ***Peri-AOF is associated with increased amyloid fibrils in select regions of the CA1 and CA3,***
248 ***but not in the dentate gyrus, in 5xFAD mice.***
249 AD dementia is more prevalent in women and may emerge at the onset of menopause. However,
250 there is limited evidence that Aβ levels in the hippocampus, which are a hallmark of AD, are
251 influenced by perimenopause. To evaluate whether Aβ increases in the hippocampus of females
252 at a stage of early ovarian failure, 5xFAD females were treated with VCD, or sesame oil as a
253 control, and Aβ levels quantified at peri-AOF, a stage corresponding to human perimenopause.
254 To obtain a more granular understanding of perimenopause role on AD pathology, analysis was
255 performed across major hippocampal subregions. Given the small size and complex geometric
256 borders of these hippocampal subregions, ELISA and similar methods requiring precise tissue
257 punches were not feasible. Instead, we employed light microscopic immunohistochemistry.
258 The density of 4G8, a marker of Aβ, was examined in CA1, CA3, DG and subicular
259 subregions in rostral and caudal hippocampal sections of the 5xFAD mice **(Fig. 2A-B**). No
260 immunoreactivity was detected in the WT mice. As described below, 4G8 labeling in the 5xFAD
261 mice varied across hippocampal subregions with sublayer specificity.
262

263 **CA1 and subiculum:** In the rostral CA1, dense 4G8-immunoreactivity (ir) was found in the
264 pyramidal cell layer (PCL), with scattered clusters in the other laminae, particularly in the stratum
265 oriens (SO) (**Fig. 2C-E**). In the rostral CA1 PCL, 5xFAD male mice exhibited lower 4G8 labeling
266 than both 5xFAD-oil treated and 5xFAD VCD-treated female mice following post-hoc analysis
267 (F=5.080, p=0.013) **(Fig. 2F)**. Similarly, in the stratum radiatum (nSR), 5xFAD males showed
268 lower 4G8 labeling compared to 5xFAD-oil treated female mice (F= 3.783, p = 0.034) **(Fig. 2F)**.
269 Analogously, in the deep stratum radiatum (dSR), the density of 4G8 labeling following post-hoc
270 analysis was lower in 5xFAD male mice compared to 5xFAD oil- and 5xFAD VCD-treated female
271 mice (F= 4.178, p = 0.025) **(Fig. 2F)**. The 4G8 labeling in the caudal CA1 was similar to that seen
272 rostrally. Moreover, scattered 4G8-positive cells were found in the subiculum though no significant
273 effects were found (Suppl. Fig. 1A-D).
274
275 **CA3:** Scattered 4G8-labeled cells were found in the PCL of CA3a and CA3b, with labeled clusters
276 dispersed throughout other laminae (**Fig. 2G-I**). No significant difference in 4G8 density was
277 observed in any sublayers of CA3a (Suppl. Fig. 1E-H). However, in the CA3b PCL, 5xFAD VCD
278 females showed greater 4G8 labeling than both 5xFAD oil-treated females and 5xFAD male mice
279 following post hoc analysis (F=5.049, p = 0.013) **(Fig. 2J)**. Additionally, in the stratum lucidum
280 (SLu) of CA3b, 5xFAD VCD-treated females showed higher 4G8 density than 5xFAD males (F =
281 5.98, p = 0.007; t(20) = 3.374, p = 0.003) **(Fig. 2J)**.
282
283 **Dentate Gyrus (DG):** In both the rostral and caudal DG, 4G8-labeling appeared in clusters
284 throughout all laminae, especially in the hilus. No significant difference in 4G8 density was
285 observed in any DG sublayers (Suppl. Fig. 1I-P).
286
287 ***Peri-AOF is associated with increased levels of reactive astrocytes in select regions of***
288 ***the rostral CA1,DG, and caudal CA1 of 5xFAD mice.***
289 Astrocytes facilitate the removal of Aβ from the brain parenchyma by mediating efflux into the
290 cerebral vasculature [67]. Their function is influenced by sex, partly through the actions of
291 estrogen signaling via its estrogen receptors [68-70]. Therefore, astrocytes are expected to play
292 an important role in amyloidosis during ovarian failure. However, evidence is limited regarding
293 changes in astrocyte activity across hippocampal subregions in both intact and reproductively
294 compromised females.
295 To assess astrocyte activation, the density of the astrocytic marker GFAP was examined
296 in CA1, CA3, DG and subicular subregions within rostral and caudal hippocampus **(Fig. 3A-B**) of

297 WT and 5xFAD oil- and VCD-treated female mice, as well as oil-treated male mice. Consistent
298 with our prior studies [58, 59], GFAP-labeled cells were found throughout all lamina of CA1, CA3
299 and DG, with fewer GFAP-positive cells in the pyramidal and granule cell layers **(Figs. 3,4).**
300 Representative micrographs of GFAP labeling are shown for rostral CA1 (**Fig. 3C-H**), caudal
301 CA1/subiculum (**Fig. 3J-O**), rostral DG (**Fig. 4A-F**), and caudal DG (**Fig. 4H-M**).
302
303 **CA1 and subiculum:** In the rostral CA1 SO region, there was a significant main effect of genotype
304 ($F_{genotype}$ = 18.50, $p < 0.0001$) and treatment ($F_{treatment}$ = 3.770, $p = 0.029$). Post-hoc analysis
305 showed that the density of GFAP labeling in SO was greater ($p < 0.05$) in 5xFAD mice than their
306 WT counterparts **(Fig. 3I)**. In the PCL region, a significant main effect of treatment was found
307 ($F_{treatment}$ = 4.822, $p = 0.011$),with WT-VCD mice showing greater GFAP labeling than WT male
308 mice ($p = 0.048$) **(Fig. 3I)**. In the SLM region, a significant main effect of genotype was observed
309 ($F_{genotype}$ = 12.20, $p = 0.0009$), and post-hoc analysis showed that 5xFAD male mice had
310 significantly greater GFAP labeling than WT male mice ($p = 0.006$) **(Fig. 3I)**.
311 In the caudal CA1 SO region, there was a significant main effect of genotype ($F_{genotype}$ =
312 38.26, $p < 0.0001$). Post-hoc analysis showed increased GFAP labeling in 5xFAD mice compared
313 to WT controls ($p < 0.05$) **(Fig. 3P)**. In the PLC region, a main effect of genotype was also
314 observed ($F_{genotype}$ = 7.458, $p = 0.008$). Post-hoc multiple comparisons showed that WT-VCD mice
315 had greater GFAP labeling than WT-oil mice ($p = 0.022$) **(Fig. 3P)**. Additionally, 5xFAD-oil mice
316 had significant higher GFAP labeling in the PLC than WT-oil mice ($p = 0.001$) **(Fig. 3P)**. In the SR
317 region, of caudal CA1, a significant main effect of genotype was observed ($F_{genotype}$ = 9.803, $p =$
318 0.003), with increased GFAP labeling in 5xFAD-oil compared to WT-oil mice ($p = 0.005$) **(Fig.**
319 **3P)**. In the SLM region, there was a significant main effect of genotype ($F_{genotype}$ = 12.49, $p =$
320 0.001), with 5xFAD-oil mice exhibiting greater GFAP labeling than WT-oil mice ($p = 0.0071$), and
321 5xFAD-male showing increased GFAP compared to WT-male mice ($p = 0.0243$) **(Fig. 3P)**. Similar
322 to other regions of caudal CA1, in the subiculum, a significant main effect of genotype was found
323 ($F_{genotype}$ = 61.46, $p < 0.0001$), with post-hoc comparisons revealing greater GFAP labeling in
324 5xFAD mice compared to WT controls ($p < 0.05$) **(Fig. 3P)**. Additionally, 5xFAD-oil mice had
325 significantly higher GFAP labeling in the subiculum than 5xFAD-male mice ($p = 0.045$) **(Fig. 3P)**.
326
327 **CA3:** No significant effect of treatment or genotype on GFAP density was observed in any CA3
328 subregions (Suppl. Fig. 2A-N).
329

330 **DG:** In the rostral DG crest, there was a significant effect of genotype ($F_{genotype}$ = 6.914, p = 0.011)
331 on the density of GFAP labeling. Post-hoc analysis revealed significantly greater GFAP labeling
332 in 5xFAD-VCD compared to WT-VCD mice (p = 0.021) (**Fig. 4G**). In the hilus, a significant main
333 effect of genotype was observed ($F_{genotype}$ = 12.21, p = 0.001), with post-hoc multiple comparison
334 analysis revealing that 5xFAD-VCD and 5xFAD-male mice had greater GFAP labeling than their
335 WT counterparts (p < 0.05) (**Fig. 4G**).
336 In the caudal DG crest, there was a significant main effect of genotype ($F_{genotype}$ = 5.325,
337 p = 0.025), with increased GFAP in 5xFAD-male compared to WT-male mice (p = 0.034) (**Fig.**
338 **4N)**. In the hilus, a main effect of genotype was also found ($F_{genotype}$ = 10.18, p = 0.002), with
339 5xFAD-male mice exhibiting greater GFAP labeling than WT-male mice (p = 0.036) (**Fig. 4N)**. In
340 the db region of the DG, a main effect of genotype was observed ($F_{genotype}$ = 18.47, p < 0.0001),
341 with increased GFAP labeling in 5xFAD-oil compared to WT-oi mice (p = 0.002) (**Fig. 4N**).
342 Similarly to the crest and hilus, 5xFAD-male mice showed significantly more GFAP labeling than
343 WT-male mice (p = 0.031) in the db (**Fig. 4N**).
344 These patterns of GFAP labeling suggest that peri-AOF is associated with increased
345 astrocyte activity in select hippocampal regions of the rostral and caudal CA1 and DG.
346
347 ***Increased microglia activation in select regions of the CA1 and DG of 5xFAD mice***
348 Microglia, the brain's resident macrophage, regulate neuroinflammation and cognitive function
349 [71]. The protein Iba1 is constitutively expressed in microglia and upregulated upon activation
350 [72, 73], a common feature of aging and neurodegenerative disorders [74]. Significantly, microglia
351 activity is influenced by ovarian hormone changes. Ovariectomy increases Iba1 expression in
352 middle-aged female mice [75], while estradiol reduces microglia reactivity in the hippocampus of
353 aged ovariectomized animals [76]. Additionally, ovariectomy elevates macrophage antigen
354 complex-1, another marker of reactive microglia, in the hippocampus of aged mice [77]. In AD
355 mouse models, chronic estrogen deficiency is linked to heightened microglial activation and
356 neurodegeneration [78]. Given these findings, ovarian failure may alter hippocampal Iba1
357 expression during amyloidosis, however, direct evidence remains limited.
358 The density of Iba1 was examined in CA1, CA3, DG and subiculum subregions within the
359 rostral and caudal hippocampus **(Fig. 5A-B**). Consistent with our prior studies [58, 59], Iba1-
360 labeled cells were scattered throughout all lamina in the CA1, CA3 and DG; however, the
361 pyramidal and granule cell layers contained less Iba1 labeling (**Figs. 5 & 6**). Representative
362 micrographs show the distribution of Iba1 labeling in the rostral CA1 **(Fig. 5C-H)**, caudal
363 CA1/subiculum **(Fig. 5J-O)**, rostral DG (**Fig. 6A-F**), and caudal DG (**Fig. 6H-M**).

364
365 **CA1 and subiculum:** In the rostral CA1 SO region, there was a significant main effect of genotype
366 ($F_{genotype}$ = 10.16, p = 0.0023) on Iba1 labeling. Post-hoc analysis showed that Iba1 density was
367 greater ($p < 0.05$) in 5xFAD-VCD and 5xFAD-male than their WT counterparts (**Fig. 5I**). In the
368 PCL region, there was a main effect of genotype ($F_{genotype}$ = 14.12, p = 0.0004) and treatment
369 ($F_{treatment}$ = 3.449, p = 0.038) on Iba1 labeling. As in the SO region, post-hoc analysis showed
370 increased labeling in 5xFAD-VCD and 5xFAD-male mice ($p < 0.05$) compared to WT mice (**Fig.**
371 **5I**). Additionally, 5xFAD-VCD mice exhibited significantly more Iba1 labeling compared to 5xFAD-
372 oil, mice (p = 0.016) **(Fig. 5I**). In the SLM region of the rostral CA1, a main effect of genotype was
373 observed ($F_{genotype}$ = 10.89, p = 0.002), with post-hoc analysis showing significantly more Iba1
374 labeling in 5xFAD-male mice than WT-male mice (p = 0.006) (**Fig. 5I**).
375 In the caudal CA1 SO region, there was a significant main effect of genotype ($F_{genotype}$ =
376 19.61, $p < 0.0001$). Post-hoc analysis showed that Iba1 density was greater ($p < 0.05$) in 5xFAD-
377 VCD and 5xFAD-male mice than their WT counterparts (**Fig. 5P**). In the PCL region, a main effect
378 of genotype ($F_{genotype}$ = 30.99, $p < 0.0001$) and treatment ($F_{treatment}$ = 4.272, p = 0.014) was
379 observed . Multiple comparisons revealed significantly more Iba1 labeling in 5xFAD mice than in
380 WT mice ($p < 0.05$) (**Fig. 5P**). Additionally, 5xFAD-VCD mice exhibited greater Iba1 labeling in
381 the PLC than 5xFAD-male mice, (p = 0.014) (**Fig. 5P**). In the SR region of the caudal CA1, a main
382 effect of genotype ($F_{genotype}$ = 9.983, p = 0.003) was found, with post-hoc analysis showing
383 significantly more Iba1 in 5xFAD-male mice than in WT-male mice (**Fig. 5P**). In the SLM, there
384 was also a main effect of genotype ($F_{genotype}$ = 14.19, p = 0.0004), with 5xFAD-male mice exhibiting
385 greater Iba1 labeling than WT-male mice **(Fig. 5P**). Similarly, in the subiculum, a significant main
386 effect of genotype ($F_{genotype}$ = 67.47, $p < 0.0001$) and treatment ($F_{treatment}$ = 3.996, p = 0.024) was
387 found, with post-hoc analysis revealing significantly more Iba1 labeling in 5xFAD mice than WT
388 mice ($p < 0.05$) **(Fig. 5P)**.
389
390 **CA3:** There was no effect of treatment or genotype on the density of Iba1 labeling in any of the
391 sublayers of CA3a or CA3b (Suppl. Fig. 2O-AB).
392
393 **DG:** In the rostral DG, there was a significant main effect of genotype ($F_{genotype}$ = 9.923, p = 0.0025)
394 on Iba1 labeling in the crest. Post-hoc analysis showed greater Iba1 density ($p < 0.05$) in 5xFAD-
395 VCD and 5xFAD-male mice than in WT mice (**Fig. 6G**). In the hilus, there was a main effect of
396 genotype ($F_{genotype}$ = 20.20, $p < 0.0001$) and treatment ($F_{treatment}$ = 4.349, p = 0.017). Post-hoc
397 analysis showed significantly more Iba1 labeling ($p < 0.05$) in 5xFAD-VCD and 5xFAD-male mice

398 compared to their WT counterparts (**Fig. 6G**). Additionally, 5xFAD-VCD mice exhibited increased
399 Iba1 density compared to 5xFAD-oil mice ($p = 0.036$) and 5xFAD-male mice ($p = 0.027$) (**Fig.**
400 **6G**). In the db of the rostral DG, a main effect of genotype ($F_{genptype} = 16.39$, $p = 0.0002$) was
401 observed, with post-hoc analysis showing greater density of Iba1 ($p < 0.05$) in 5xFAD-VCD and
402 5xFAD-male mice compared to WT mice (**Fig. 6G**).
403 In the caudal DG, a main effect of genotype ($F_{genotype} = 10.04$, $p = 0.002$) was found in the
404 crest, with 5xFAD males exhibiting greater Iba1 density than WT male mice ($p = 0.003$) (**Fig. 6N**).
405 In the caudal hilus, a significant main effect of genotype ($F_{genotype} = 20.42$, $p < 0.0001$) was
406 observed, with post-hoc analysis showing greater Iba1 labeling ($p < 0.05$) in 5xFAD mice than in
407 their WT counterparts (**Fig. 6N**). Similarly, a significant main effect of genotype ($F_{genotype} = 25.07$,
408 $p < 0.0001$) was determined in the db of the DG, with multiple comparisons revealing significantly
409 more Iba1-labeling ($p < 0.01$) in 5xFAD mice than in WT mice (**Fig. 6N**).
410
411 These results suggest that the 5xFAD genotype at peri-AOF influences microglia
412 activation in multiple subregions of rostral and caudal CA1and DG compared to peri-AOF WT
413 mice. Additionally, peri-AOF further exacerbates microglia activation in 5xFAD mice in rostral CA1
414 PCL and DG hilus, suggesting sex-dependent vulnerability. These findings, in concert with
415 increased GFAP labeling in select hippocampal regions, suggest enhanced susceptibility to
416 neuroinflammation at the intersection of AD and perimenopause.
417
418 ***Cognitive impairment varies with genotype, sex and AOF***
419 Neuroinflammation is intrinsically linked to the progression of cognitive impairment and dementia
420 [79]. However, the impact of early ovarian failure on cognitive function in VCD-treated 5xFAD
421 mice, and how this compares to males, remains unknown. To address this, we assessed the
422 behavioral consequences of early ovarian decline in 5xFAD mice compared to non-VCD treated
423 females and males using different cognitive tests sensitive to Aβ pathology, including the Y-maze
424 alternation test, novel object recognition, and spatial navigation in the Barnes maze.
425
426 **Y-maze:** No significant differences were observed in arm alternation behavior (**Fig. 7A**) or in the
427 total number of arm entries in all 3 arms during the testing period (**Fig. 7B**) between 5xFAD and
428 WT mice. No differences were observed in the % novel arm entries respect to total arm entries
429 and in the time spent in the novel arm (data not shown). This may suggest preservation of short-
430 term working memory or that other cognitive domains might be more affected in 5xFAD mice and
431 in VCD-treated females at a young age.

Novel object: An effect of AOF was seen in locomotor activity as assessed by total distance travelled ($F(5, 60) = 2.42$, $p = 0.05$). 5xFAD-male compared to 5xFAD-VCD female mice had a lower total distance ($p = 0.06$), although not significant **(Fig. 7C)**. No significant differences across groups were observed in the total object exploration time or in Novel Object Recognition Index **(Fig. 7D-E)**. Interestingly, significant increase in time spent exploring the novel object vs. the familiar object was observed between WT-male ($p < 0.0001$) and 5xFAD-male mice ($p = 0.001$) **(Fig. 7F)**. For females, significant differences in time spent exploring familiar and novel objects were found between treatment in WT mice (WT-female ($p = 0.018$); WT-VCD female ($p = 0.014$)), but did not extend to 5xFAD females **(Fig. 7F)**.

Barnes maze: There were no significant differences in motor activity, as assessed by distance traveled and mean speed between 5xFAD and WT mice, regardless of genotype or treatment (**Fig. 8A-B**). Although, a significance difference was observed in mean speed between WT females and VCD-treated WT females at day 1 only ($p=0.0086$). Also, no differences were observed in learning measures as shown for latency to find the escape and path efficiency (**Fig. 8C-D**) .When cognitive performance was tested 24 hrs after the final acquisition training session, VCD-treated WT-females spent significantly less time in the target quadrant where the escape hole was located, and more time in non-target quadrants compared to both WT-oil or 5xFAD-VCD females **(Fig. 8E-F)**. Given that the Barnes maze is a measure of spatial learning and memory, the altered performance in VCD-treated WT females suggests a potential adverse effect of early ovarian failure on spatial memory. This effect appears to be mitigated in 5xFAD-VCD females.

Overall, these behavioral data demonstrate that VCD treatment impairs performance in select cognitive tasks. Combined with our anatomical findings on Aβ deposition and glia activation in the hippocampus, these results suggest that early ovarian failure contributes to early-stage AD-like neurobehavioral pathology.

DISCUSSION

The relationship between early ovarian failure and neuroinflammation in the hippocampus was investigated using a model of perimenopausal AD that combined chemically-induced AOF with transgenic 5xFAD mice. Age-matched males were also tested in tandem. Mice at approximately 4-months of age showed complex effects on production of Aβ as well as signs of

466 astrocyte and microglia activity that varied by genotype, VCD treatment (AOF) and sex. We found
467 that Aβ expression was elevated in female 5xFAD mice, but only further increased in peri-AOF
468 mice in select hippocampal subregions. Further, increases in glial activation also paralleled Aβ
469 pathology but only in discrete areas of the hippocampus. Assessment of cognitive function
470 showed no effect of peri-AOF in the Y-maze, in the Novel Object Recognition tests, or across
471 Barnes Maze training days (days 1-4). Interestingly, peri-AOF reduced the time spent in the
472 Barnes Maze target quadrant during the testing day (day 5) in WT but not in 5xFAD females,
473 suggesting a treatment-genotype interaction effect. These data provide preclinical experimental
474 evidence supporting the contention that peri-menopause is a sensitive period for
475 neuroinflammation and cognitive function in women.

476 AD, the most prevalent of the dementias [2], is classically characterized by Aβ deposition
477 and cognitive impairment. However, AD also involves a complex set of neurodegenerative
478 processes, including neuroinflammation [6]. Importantly, the incidence, progression, and severity
479 of the disease are greater in women [9, 10]. Further, perimenopause may be a critical period for
480 the emergence of AD, suggesting that altered gonadal hormone levels contribute to the increased
481 AD risk [11]. Although perimenopause represents a potential turning point in AD pathology, the
482 impact of associated hormonal changes on hippocampal pathology remains unclear. To
483 investigate the role of early ovarian decline in AD pathology, we exposed female 5xFAD mice to
484 the ovotoxin VCD to induce AOF and tested them at an age when brain amyloid deposition and
485 ovarian failure are both at early stages. Age-matched WT mice and 5xFAD male mice were also
486 studied to isolate the impact of AOF independently of amyloidosis and to characterize sex
487 differences, respectively.

488 We found that Aβ expression was elevated in female 5xFAD peri-AOF mice (injected with
489 VCD) compared to intact females and males injected with sesame oil, in select hippocampal
490 subregions such as the CA1 and CA3b, but not CA3a. The mechanism underlying increased Aß
491 levels in CA3b compared to CA3a in VCD-treated 5xFAD mice is unclear at present. Presumably,
492 these regional differences are mediated by neurophysiological [80, 81], transcriptional [82, 83],
493 connectional [84], morphological [81] and functional [85] divergence across these CA3 subfields,
494 which in turn may be modulated by sex and estrogens. For example, CA3b and CA3a each show
495 unique changes in expression patterns of both stress and plasticity-related molecules following
496 stress, a modulator of dementia [86], and do so in an estrogen-dependent manner [33, 62, 87].
497 These results suggest that the pathways linking Aß pathology with estrogen signaling within the
498 CA3 are subregion-specific, and further research is needed to clarify their specific contributions
499 to learning and memory during ovarian failure. In VCD-injected WT mice, GFAP density was

500 increased compared to oil-treated WT mice in the caudal CA1 PCL and compared to males in the
501 rostral CA1 PCL. No differences were detected with regard to Iba-1 labeling in any hippocampal
502 region between the WT mice. The increased astrogliosis observed during peri-AOF may result
503 from the loss of astrocyte estrogen signaling. Both resting and activated astrocytes are prominent
504 among the non-neuronal hippocampal cell types that express estrogen receptors alpha and beta
505 [88-90] as well as G-protein estrogen receptors [91]. Further, the expression and cellular location
506 of estrogen receptors in the hippocampus are influenced by estrogen levels [92, 93]. Estrogen
507 modulates GFAP expression [94] and regulates the expression of genes involved in astrocyte
508 proliferation [95]. Importantly, the CA1 PCL is an estrogen receptor-expressing region of the
509 hippocampus [88-90] and is a major hippocampal output that plays a critical role in both spatial
510 and non-spatial memory processes [96]. The functional impact of elevated astrocyte activation in
511 the context of reduced estrogen signaling remains unclear, although it may involve the loss of
512 estrogen-mediated neuroprotection and/or the activation of compensatory mechanisms . This is
513 supported by findings that estrogen reduces glucose- and oxygen-deprivation-induced apoptosis
514 in astrocyte-neuron co-cultures, and that estrogen replacement attenuates the increased
515 apoptosis in the CA1 produced by cerebral ischemia [97]. Given the protective role of estrogen
516 against astrocytosis-associated neural dysfunction, its loss in the CA1 PCL region suggests an
517 increased vulnerability to stress or insult and a heightened propensity for neural pathology.
518 In addition to their critical metabolic role, astrocytes exert important effects on neuronal
519 signaling and plasticity, particularly via modulation of pyramidal cells [98, 99]. CA1 pyramidal cell
520 hyperexcitability is a hallmark of neurodegeneration and, in particular, is observed in AD models
521 [100-102]. Significantly, astrocytes contribute to CA1 pyramidal cell activity [103-105], and
522 reactive astrocytes are associated with decreased inhibitory synaptic currents and CA1
523 hyperexcitability [106]. Thus, increased astrocyte activity in the CA1 PCL during early AOF, in the
524 context of disrupted estrogen signaling, may contribute to conditions favoring pyramidal cell
525 dysfunction.
526 We examined astrogliosis and Aβ expression in peri-AOF 5xFAD mice. Compared to WT
527 VCD-treated mice, 5xFAD VCD mice did not show a further increase in GFAP in the CA1 PCL.
528 However, GFAP density was increased in the CA1 SO and subiculum in VCD-treated 5xFAD mice
529 compared to similarly treated WT mice. Additionally, 5xFAD peri-AOF mice showed higher GFAP
530 density in the crest and hilus of the rostral DG compared to WT mice.
531 Microglia activation was also observed. Iba-1 levels were higher in peri-AOF 5xFAD mice
532 compared to peri-AOF WT mice in the CA1 PCL, SO and subiculum as well as the different
533 subregions of the DG These results indicate that microglia are recruited in non-pyramidal cell

534 regions of the CA1. Significantly, microglia activation was greater in CA1 PCL and DG hilus cells
535 in 5xFAD peri-AOF mice compared to 5xFAD females and males.
536 The increased 4G8 density observed in 5xFAD mice was expected to be coupled with
537 elevated GFAP and Iba-1 levels. We found that in VCD-treated mice only the CA3b PCL showed
538 increased Aβ compared to both oil-treated female and male controls. However, there were no
539 differences in either GFAP or Iba-1 across any treatment in any CA3 field. Additionally, in both
540 oil and VCD 5xFAD mice, 4G8 in the CA1 PCL was higher compared to males. Yet, this was
541 associated with increased Iba-1 only in peri-AOF mice, suggesting that this region may be
542 particularly sensitive in response to AOF and Aβ aggregation. The lack of coupling between
543 increased neuroinflammatory markers and Aβ levels in several hippocampal subregions suggests
544 that peri-AOF affects glial activity independently of amyloid aggregation in these areas. Alterations
545 in brain function have been described prior to Aβ plaque or fibril formation in other APP
546 overexpressing mouse models [107]. For example, functional hyperemia is impaired in young
547 mice prior to Aβ aggregation [107] and deficits in autoregulation occur [108]. These effects may
548 be attributed to the actions of soluble oligomeric Aβ [109], which are detectable in 5xFAD mice at
549 the age range studied here [110]. Notably, oligomeric Aβ can impact astrocytes [111] and
550 microglia [112].
551 Our findings in 5xFAD mice contrast with similar experiments in SwDI mice, a model of
552 cerebral amyloid angiopathy [42, 113]. In SwDI VCD mice, we found increased 4G8 in the CA1
553 SO and DG. Further, astrocyte and microglia activation was observed in the CA1 SO, and
554 astrocytes in the DG crest. Pyramidal cell layers of the CA1 and CA3 were not affected. These
555 results indicate that dementia models with Aβ pathology in either parenchyma or cerebral
556 vasculature exhibit distinct patterns of hippocampal amyloid deposition and glial cell activation
557 with notable differences in pyramidal and non-pyramidal regions.
558 The present results demonstrate that distinct hippocampus regions exhibit differential
559 susceptibility to AOF and Aβ in 5xFAD mice. The CA1 of 5xFAD mice, particularly the pyramidal
560 cell layer, was vulnerable to the neuroinflammatory effects of peri-AOF. This aligns with evidence
561 that the CA1 is the earliest hippocampal subregion to exhibit neuronal loss in AD [114, 115] and
562 that astrocyte-pyramidal cell interactions in the CA1 are disrupted in AD models [116].
563 Interestingly, the pyramidal cell layer of the CA3b region uniquely demonstrated elevated
564 Aβ in 5xFAD peri-AOF mice. The CA3 is a region that expresses estrogen receptors [88, 117-
565 120], contains estrogen-sensitive neurons [33], and may be protected against Aβ-mediated
566 degeneration by estrogen [121]. Together with our findings in WT mice, these results suggest that

pyramidal cell layers of the CA1 and CA3 fields are particularly sensitive to decreased estrogen and increased Aβ during early AOF in female mice. In sum, these findings highlight the complex interplay between ovarian hormone loss, neuroinflammation, and amyloid pathology, underscoring the need for further research into the mechanisms by which perimenopause contributes to heightened AD susceptibility in women.

ACKNOWLEDGEMENTS: Supported by NIH grants R01 HL136520 and HL13650S1 (TAM & MJG), R01 HL135428 (MJG), R01 GM130722 (JP), R21 AG064455 (RM), R01 NS097805 (LP).

Author contributions: Conceptualization: TAM, MJG, RM, JP, LP; Formal analysis: GS, FY, CW Investigation: GS, FY, TAM, MJG; Resources: TAM, MJG, LP; Writing – original draft preparation: MGJ, TAM, RM, JP; writing - review & editing: GS, RM, JP, MGJ, TAM; visualization: FY, GS; supervision: TAM, MJG; project administration: TAM, MJG; funding acquisition: MJG, TAM, LP.

REFERENCES

[1] "2023 Alzheimer's disease facts and figures," (in eng), *Alzheimers Dement,* vol. 19, no. 4, pp. 1598-1695, Apr 2023, doi: 10.1002/alz.13016.

[2] A. Alzheimer's, "Alzheimer's disease facts and figures," *Alzheimers Dement.,* vol. 12, pp. 459-509, 2016.

[3] Z. Arvanitakis, R. C. Shah, and D. A. Bennett, "Diagnosis and Management of Dementia: Review," (in eng), *Jama,* vol. 322, no. 16, pp. 1589-1599, Oct 22 2019, doi: 10.1001/jama.2019.4782.

[4] J. Zhang, Y. Zhang, J. Wang, Y. Xia, and L. Chen, "Recent advances in Alzheimer's disease: Mechanisms, clinical trials and new drug development strategies," (in eng), *Signal Transduct Target Ther,* vol. 9, no. 1, p. 211, Aug 23 2024, doi: 10.1038/s41392-024-01911-3.

[5] H. Braak and E. Braak, "Neuropathological stageing of Alzheimer-related changes," (in eng), *Acta Neuropathol,* vol. 82, no. 4, pp. 239-59, 1991, doi: 10.1007/bf00308809.

[6] S. Lista *et al.*, "Tracking neuroinflammatory biomarkers in Alzheimer's disease: a strategy for individualized therapeutic approaches?," (in eng), *J Neuroinflammation,* vol. 21, no. 1, p. 187, Jul 30 2024, doi: 10.1186/s12974-024-03163-y.

[7] L. Raz, J. Knoefel, and K. Bhaskar, "The neuropathology and cerebrovascular mechanisms of dementia," (in eng), *J Cereb Blood Flow Metab,* vol. 36, no. 1, pp. 172-86, Jan 2016, doi: 10.1038/jcbfm.2015.164.

[8] Z. Kolahchi *et al.*, "Sex and Gender Differences in Alzheimer's Disease: Genetic, Hormonal, and Inflammation Impacts," (in eng), *Int J Mol Sci,* vol. 25, no. 15, Aug 3 2024, doi: 10.3390/ijms25158485.

[9] C. J. Pike, "Sex and the development of Alzheimer's disease," *J. Neurosci. Res.,* vol. 95, pp. 671–680, 2017.

[10] K. R. Laws, K. Irvine, and T. M. Gale, "Sex differences in cognitive impairment in Alzheimer's disease," *World J. Psychiatry* vol. 6, pp. 54–65, 2016.

[11] J. Gong, K. Harris, S. A. E. Peters, and M. Woodward, "Reproductive factors and the risk of incident dementia: A cohort study of UK Biobank participants," (in eng), *PLoS Med,* vol. 19, no. 4, p. e1003955, Apr 2022, doi: 10.1371/journal.pmed.1003955.

[12] H. Liao *et al.*, "Association of earlier age at menopause with risk of incident dementia, brain structural indices and the potential mediators: a prospective community-based cohort study," (in eng), *EClinicalMedicine,* vol. 60, p. 102033, Jun 2023, doi: 10.1016/j.eclinm.2023.102033.

[13] Y. Wedatilake, C. Myrstad, S. E. Tom, B. H. Strand, S. Bergh, and G. Selbæk, "Female Reproductive Factors and Risk of Mild Cognitive Impairment and Dementia: The HUNT Study," (in eng), *J Prev Alzheimers Dis,* vol. 11, no. 4, pp. 1063-1072, 2024, doi: 10.14283/jpad.2024.46.

[14] J. J. Steventon *et al.*, "Menopause age, reproductive span and hormone therapy duration predict the volume of medial temporal lobe brain structures in postmenopausal women," (in eng), *Psychoneuroendocrinology,* vol. 158, p. 106393, Dec 2023, doi: 10.1016/j.psyneuen.2023.106393.

[15] Z. B. Mills, R. L. M. Faull, and A. Kwakowsky, "Is Hormone Replacement Therapy a Risk Factor or a Therapeutic Option for Alzheimer's Disease?," (in eng), *Int J Mol Sci,* vol. 24, no. 4, Feb 6 2023, doi: 10.3390/ijms24043205.

[16] L. Mosconi *et al.*, "Increased Alzheimer's risk during the menopause transition: A 3-year longitudinal brain imaging study," (in eng), *PLoS One,* vol. 13, no. 12, p. e0207885, 2018, doi: 10.1371/journal.pone.0207885.

[17] L. Mosconi *et al.*, "Sex differences in Alzheimer risk: Brain imaging of endocrine vs chronologic aging," (in eng), *Neurology,* vol. 89, no. 13, pp. 1382-1390, Sep 26 2017, doi: 10.1212/wnl.0000000000004425.
[18] H. Oakley *et al.*, "Intraneuronal beta-amyloid aggregates, neurodegeneration, and neuron loss in transgenic mice with five familial Alzheimer's disease mutations: potential factors in amyloid plaque formation," (in eng), *J Neurosci,* vol. 26, no. 40, pp. 10129-40, Oct 4 2006, doi: 10.1523/jneurosci.1202-06.2006.
[19] Z. Manji, A. Rojas, W. Wang, R. Dingledine, N. H. Varvel, and T. Ganesh, "5xFAD Mice Display Sex-Dependent Inflammatory Gene Induction During the Prodromal Stage of Alzheimer's Disease," (in eng), *J Alzheimers Dis,* vol. 70, no. 4, pp. 1259-1274, 2019, doi: 10.3233/jad-180678.
[20] A. Sil, A. Erfani, N. Lamb, R. Copland, G. Riedel, and B. Platt, "Sex Differences in Behavior and Molecular Pathology in the 5XFAD Model," (in eng), *J Alzheimers Dis,* vol. 85, no. 2, pp. 755-778, 2022, doi: 10.3233/jad-210523.
[21] R. Islam, R. Rajan, H. Choudhary, F. Vrionis, and K. A. Hanafy, "Gender differences in Alzheimer's may be associated with TLR4-LYN expression in damage associated microglia and neuronal phagocytosis," (in eng), *J Cell Physiol,* vol. 239, no. 6, p. e30916, Jun 2024, doi: 10.1002/jcp.30916.
[22] S. Bhattacharya, C. Haertel, A. Maelicke, and D. Montag, "Galantamine slows down plaque formation and behavioral decline in the 5XFAD mouse model of Alzheimer's disease," (in eng), *PLoS One,* vol. 9, no. 2, p. e89454, 2014, doi: 10.1371/journal.pone.0089454.
[23] A. Ganesh, W. Choudhury, and L. Coutellier, "Early spatial recognition memory deficits in 5XFAD female mice are associated with disruption of prefrontal parvalbumin neurons," (in eng), *Brain Res,* vol. 1841, p. 149122, Oct 15 2024, doi: 10.1016/j.brainres.2024.149122.
[24] T. P. O'Leary, K. R. Stover, H. M. Mantolino, S. Darvesh, and R. E. Brown, "Intact olfactory memory in the 5xFAD mouse model of Alzheimer's disease from 3 to 15 months of age," (in eng), *Behav Brain Res,* vol. 393, p. 112731, Sep 1 2020, doi: 10.1016/j.bbr.2020.112731.
[25] J. L. Bundy, C. Vied, C. Badger, and R. S. Nowakowski, "Sex-biased hippocampal pathology in the 5XFAD mouse model of Alzheimer's disease: A multi-omic analysis," (in eng), *J Comp Neurol,* vol. 527, no. 2, pp. 462-475, Feb 1 2019, doi: 10.1002/cne.24551.
[26] F. Blasco Tavares Pereira Lopes *et al.*, "Temporal and Sex-Linked Protein Expression Dynamics in a Familial Model of Alzheimer's Disease," (in eng), *Mol Cell Proteomics,* vol. 21, no. 9, p. 100280, Sep 2022, doi: 10.1016/j.mcpro.2022.100280.
[27] C. H. Poon *et al.*, "Sex Differences between Neuronal Loss and the Early Onset of Amyloid Deposits and Behavioral Consequences in 5xFAD Transgenic Mouse as a Model for Alzheimer's Disease," (in eng), *Cells,* vol. 12, no. 5, Mar 1 2023, doi: 10.3390/cells12050780.
[28] K. R. Sadleir, W. A. Eimer, S. L. Cole, and R. Vassar, "Aβ reduction in BACE1 heterozygous null 5XFAD mice is associated with transgenic APP level," (in eng), *Mol Neurodegener,* vol. 10, p. 1, Jan 7 2015, doi: 10.1186/1750-1326-10-1.
[29] C. L. Maarouf *et al.*, "Molecular Differences and Similarities Between Alzheimer's Disease and the 5XFAD Transgenic Mouse Model of Amyloidosis," (in eng), *Biochem Insights,* vol. 6, pp. 1-10, 2013, doi: 10.4137/bci.s13025.
[30] J. Prange-Kiel, D. A. Dudzinski, F. Pröls, M. Glatzel, J. Matschke, and G. M. Rune, "Aromatase Expression in the Hippocampus of AD Patients and 5xFAD Mice," (in eng), *Neural Plast,* vol. 2016, p. 9802086, 2016, doi: 10.1155/2016/9802086.
[31] T. Kubota, H. Matsumoto, and Y. Kirino, "Ameliorative effect of membrane-associated estrogen receptor G protein coupled receptor 30 activation on object recognition memory

in mouse models of Alzheimer's disease," (in eng), *J Pharmacol Sci,* vol. 131, no. 3, pp. 219-22, Jul 2016, doi: 10.1016/j.jphs.2016.06.005.

[32] J. F. Quinn *et al.*, "The novel estrogen receptor modulator STX attenuates Amyloid-β neurotoxicity in the 5XFAD mouse model of Alzheimer's disease," (in eng), *Neurobiol Dis,* vol. 174, p. 105888, Nov 2022, doi: 10.1016/j.nbd.2022.105888.

[33] T. A. Van Kempen, J. Gorecka, A. D. Gonzalez, F. Soeda, T. A. Milner, and E. M. Waters, "Characterization of neural estrogen signaling and neurotrophic changes in the accelerated ovarian failure mouse model of menopause," (in eng), *Endocrinology,* vol. 155, no. 9, pp. 3610-23, Sep 2014, doi: 10.1210/en.2014-1190.

[34] H. L. Brooks, D. P. Pollow, and P. B. Hoyer, "The VCD Mouse Model of Menopause and Perimenopause for the Study of Sex Differences in Cardiovascular Disease and the Metabolic Syndrome," (in eng), *Physiology (Bethesda),* vol. 31, no. 4, pp. 250-7, Jul 2016, doi: 10.1152/physiol.00057.2014.

[35] J. Marques-Lopes *et al.*, "Redistribution of NMDA Receptors in Estrogen-Receptor-β-Containing Paraventricular Hypothalamic Neurons following Slow-Pressor Angiotensin II Hypertension in Female Mice with Accelerated Ovarian Failure," (in eng), *Neuroendocrinology,* vol. 104, no. 3, pp. 239-256, 2017, doi: 10.1159/000446073.

[36] C. Abi-Ghanem *et al.*, "Interactions between menopause and high-fat diet on cognition and pathology in a mouse model of Alzheimer's disease," *Alzheimers Dement,* vol. 21, no. 3, p. e70026, Mar 2025, doi: 10.1002/alz.70026.

[37] C. Abi-Ghanem *et al.*, "Effects of Menopause and High Fat Diet on Metabolic Outcomes in a Mouse Model of Alzheimer's Disease," *J Alzheimers Dis,* vol. 101, no. 4, pp. 1177-1194, 2024, doi: 10.3233/JAD-231332.

[38] O. J. Gannon *et al.*, "Menopause causes metabolic and cognitive impairments in a chronic cerebral hypoperfusion model of vascular contributions to cognitive impairment and dementia," *Biol Sex Differ,* vol. 14, no. 1, p. 34, May 23 2023, doi: 10.1186/s13293-023-00518-7.

[39] M. S. Golub *et al.*, "Behavioral consequences of ovarian atrophy and estrogen replacement in the APPswe mouse," *Neurobiology of aging,* vol. 29, no. 10, pp. 1512-23, Oct 2008, doi: 10.1016/j.neurobiolaging.2007.03.015.

[40] J. A. Blackwell *et al.*, "Cerebral arteriolar and neurovascular dysfunction after chemically induced menopause in mice," *Am J Physiol Heart Circ Physiol,* vol. 323, no. 5, pp. H845-H860, Nov 1 2022, doi: 10.1152/ajpheart.00276.2022.

[41] K. Flurkey and J. M. Currer, "Pitfalls of animal model systems in ageing research," (in eng), *Best Pract Res Clin Endocrinol Metab,* vol. 18, no. 3, pp. 407-21, Sep 2004, doi: 10.1016/j.beem.2004.02.001.

[42] W. Xu *et al.*, "Cerebral microvascular rather than parenchymal amyloid-β protein pathology promotes early cognitive impairment in transgenic mice," (in eng), *J Alzheimers Dis,* vol. 38, no. 3, pp. 621-32, 2014, doi: 10.3233/jad-130758.

[43] B. C. Richard, A. Kurdakova, S. Baches, T. A. Bayer, S. Weggen, and O. Wirths, "Gene Dosage Dependent Aggravation of the Neurological Phenotype in the 5XFAD Mouse Model of Alzheimer's Disease," (in eng), *J Alzheimers Dis,* vol. 45, no. 4, pp. 1223-36, 2015, doi: 10.3233/jad-143120.

[44] W. Xu *et al.*, "Cerebral microvascular rather than parenchymal amyloid-β protein pathology promotes early cognitive impairment in transgenic mice," *J. Alzheimers Dis.,* vol. 38, pp. 621-32, 2014.

[45] T. A. Van Kempen, T. A. Milner, and E. M. Waters, "Accelerated ovarian failure: a novel, chemically induced animal model of menopause," (in eng), *Brain Res,* vol. 1379, pp. 176-87, Mar 16 2011, doi: 10.1016/j.brainres.2010.12.064.

[46] J. Marques-Lopes, Van Kempen, T.A., Milner, T.A., "Rodent Models of Ovarian Failure," in *Conn's Handbook of Models for Human Aging*, P. M. C. Jeffery Ram Ed., 2nd ed.: Elsevier Inc., 2018, ch. Chapter 60, pp. 831-843.
[47] J. R. Haas, P. J. Christian, and P. B. Hoyer, "Effects of impending ovarian failure induced by 4-vinylcyclohexene diepoxide on fertility in C57BL/6 female mice," (in eng), *Comp Med,* vol. 57, no. 5, pp. 443-9, Oct 2007.
[48] S. K. Sahambi, J. A. Visser, A. P. Themmen, L. P. Mayer, and P. J. Devine, "Correlation of serum anti-Mullerian hormone with accelerated follicle loss following 4-vinylcyclohexene diepoxide-induced follicle loss in mice," *Reprod Toxicol,* vol. 26, no. 2, pp. 116-22, Oct 2008, doi: 10.1016/j.reprotox.2008.07.005.
[49] L. E. Wright *et al.*, "Comparison of skeletal effects of ovariectomy versus chemically induced ovarian failure in mice," *J Bone Miner Res,* vol. 23, no. 8, pp. 1296-303, Aug 2008, doi: 10.1359/jbmr.080309.
[50] J. C. Lohff, P. J. Christian, S. L. Marion, A. Arrandale, and P. B. Hoyer, "Characterization of cyclicity and hormonal profile with impending ovarian failure in a novel chemical-induced mouse model of perimenopause," *Comp Med,* vol. 55, no. 6, pp. 523-7, Dec 2005. [Online]. Available: http://www.ncbi.nlm.nih.gov/pubmed/16422148.
[51] L. P. Mayer, P. J. Devine, C. A. Dyer, and P. B. Hoyer, "The follicle-deplete mouse ovary produces androgen," (in eng), *Biol Reprod,* vol. 71, no. 1, pp. 130-8, Jul 2004, doi: 10.1095/biolreprod.103.016113.
[52] V. Harsh, P. J. Schmidt, and D. R. Rubinow, "The menopause transition: the next neuroendocrine frontier," (in eng), *Expert Rev Neurother,* vol. 7, no. 11 Suppl, pp. S7-10, Nov 2007, doi: 10.1586/14737175.7.11s.S7
10.1586/14737175.7.11s.S7.
[53] C. D. Turner and J. T. Bagnara, *General Endocrinology*. Philadelphia: W.B. Saunders, 1971.
[54] E. Kövari, F. R. Herrmann, P. R. Hof, and C. Bouras, "The relationship between cerebral amyloid angiopathy and cortical microinfarcts in brain ageing and Alzheimer's disease," (in eng), *Neuropathol Appl Neurobiol,* vol. 39, no. 5, pp. 498-509, Aug 2013, doi: 10.1111/nan.12003.
[55] I. Alafuzoff *et al.*, "Assessment of beta-amyloid deposits in human brain: a study of the BrainNet Europe Consortium," (in eng), *Acta Neuropathol,* vol. 117, no. 3, pp. 309-20, Mar 2009, doi: 10.1007/s00401-009-0485-4.
[56] P. Marazuela, B. Paez-Montserrat, A. Bonaterra-Pastra, M. Solé, and M. Hernández-Guillamon, "Impact of Cerebral Amyloid Angiopathy in Two Transgenic Mouse Models of Cerebral β-Amyloidosis: A Neuropathological Study," (in eng), *Int J Mol Sci,* vol. 23, no. 9, Apr 29 2022, doi: 10.3390/ijms23094972.
[57] J. Davis *et al.*, "Early-onset and robust cerebral microvascular accumulation of amyloid beta-protein in transgenic mice expressing low levels of a vasculotropic Dutch/Iowa mutant form of amyloid beta-protein precursor," (in eng), *J Biol Chem,* vol. 279, no. 19, pp. 20296-306, May 7 2004, doi: 10.1074/jbc.M312946200.
[58] T. A. Milner *et al.*, "Angiotensin II differentially affects hippocampal glial inflammatory markers in young adult male and female mice," (in eng), *Learn Mem,* vol. 29, no. 9, pp. 265-273, Sep 2022, doi: 10.1101/lm.053507.121.
[59] J. Platholi *et al.*, "Hippocampal glial inflammatory markers are differentially altered in a novel mouse model of perimenopausal cerebral amyloid angiopathy," (in eng), *Front Aging Neurosci,* vol. 15, p. 1280218, 2023, doi: 10.3389/fnagi.2023.1280218.
[60] T. A. Milner, E. M. Waters, D. C. Robinson, and J. P. Pierce, "Degenerating processes identified by electron microscpic immunocytochemical methods," in *Neurodegeneration, Methods and Protocols*, G. Manfredi and H. Kawamata Eds. New York: Springer, 2011, pp. 23-59

[61] P. Hof, W. Young, F. Bloom, P. Belinchenko, and M. Ceilo, *Comparative cytoarchitectonic atlas of the C57BL/6 and 129/SV mouse brains*, 1 ed. Amsterdam: Elsevier, 2000.
[62] J. P. Pierce, D. T. Kelter, B. S. McEwen, E. M. Waters, and T. A. Milner, "Hippocampal mossy fiber leu-enkephalin immunoreactivity in female rats is significantly altered following both acute and chronic stress," (in eng), *J Chem Neuroanat,* vol. 55, pp. 9-17, Jan 2014, doi: 10.1016/j.jchemneu.2013.10.004.
[63] T. J. Williams and T. A. Milner, "Delta opioid receptors colocalize with corticotropin releasing factor in hippocampal interneurons," (in eng), *Neuroscience,* vol. 179, pp. 9-22, Apr 14 2011, doi: 10.1016/j.neuroscience.2011.01.034.
[64] T. J. Williams, A. Torres-Reveron, J. D. Chapleau, and T. A. Milner, "Hormonal regulation of delta opioid receptor immunoreactivity in interneurons and pyramidal cells in the rat hippocampus," (in eng), *Neurobiology of learning and memory,* vol. 95, no. 2, pp. 206-20, Feb 2011, doi: 10.1016/j.nlm.2011.01.002.
[65] L. Park *et al.*, "Tau induces PSD95-neuronal NOS uncoupling and neurovascular dysfunction independent of neurodegeneration," (in eng), *Nat Neurosci,* vol. 23, no. 9, pp. 1079-1089, Sep 2020, doi: 10.1038/s41593-020-0686-7.
[66] L. Park *et al.*, "Nox2-derived radicals contribute to neurovascular and behavioral dysfunction in mice overexpressing the amyloid precursor protein," (in eng), *Proc Natl Acad Sci U S A,* vol. 105, no. 4, pp. 1347-52, Jan 29 2008, doi: 10.1073/pnas.0711568105.
[67] C. Y. Liu, Y. Yang, W. N. Ju, X. Wang, and H. L. Zhang, "Emerging Roles of Astrocytes in Neuro-Vascular Unit and the Tripartite Synapse With Emphasis on Reactive Gliosis in the Context of Alzheimer's Disease," (in eng), *Front Cell Neurosci,* vol. 12, p. 193, 2018, doi: 10.3389/fncel.2018.00193.
[68] M. Santos-Galindo, E. Acaz-Fonseca, M. J. Bellini, and L. M. Garcia-Segura, "Sex differences in the inflammatory response of primary astrocytes to lipopolysaccharide," (in eng), *Biol Sex Differ,* vol. 2, p. 7, Jul 11 2011, doi: 10.1186/2042-6410-2-7.
[69] J. A. Chowen and L. M. Garcia-Segura, "Role of glial cells in the generation of sex differences in neurodegenerative diseases and brain aging," (in eng), *Mech Ageing Dev,* vol. 196, p. 111473, Jun 2021, doi: 10.1016/j.mad.2021.111473.
[70] Y. Lu *et al.*, "Neuron-Derived Estrogen Is Critical for Astrocyte Activation and Neuroprotection of the Ischemic Brain," (in eng), *J Neurosci,* vol. 40, no. 38, pp. 7355-7374, Sep 16 2020, doi: 10.1523/jneurosci.0115-20.2020.
[71] J. Cornell, S. Salinas, H. Y. Huang, and M. Zhou, "Microglia regulation of synaptic plasticity and learning and memory," (in eng), *Neural Regen Res,* vol. 17, no. 4, pp. 705-716, Apr 2022, doi: 10.4103/1673-5374.322423.
[72] Y. Sasaki, K. Ohsawa, H. Kanazawa, S. Kohsaka, and Y. Imai, "Iba1 is an actin-cross-linking protein in macrophages/microglia," (in eng), *Biochem Biophys Res Commun,* vol. 286, no. 2, pp. 292-7, Aug 17 2001, doi: 10.1006/bbrc.2001.5388.
[73] Y. Imai, I. Ibata, D. Ito, K. Ohsawa, and S. Kohsaka, "A novel gene iba1 in the major histocompatibility complex class III region encoding an EF hand protein expressed in a monocytic lineage," (in eng), *Biochem Biophys Res Commun,* vol. 224, no. 3, pp. 855-62, Jul 25 1996, doi: 10.1006/bbrc.1996.1112.
[74] M. Prinz, T. Masuda, M. A. Wheeler, and F. J. Quintana, "Microglia and Central Nervous System-Associated Macrophages-From Origin to Disease Modulation," (in eng), *Annu Rev Immunol,* vol. 39, pp. 251-277, Apr 26 2021, doi: 10.1146/annurev-immunol-093019-110159.
[75] M. Sárvári, I. Kalló, E. Hrabovszky, N. Solymosi, and Z. Liposits, "Ovariectomy Alters Gene Expression of the Hippocampal Formation in Middle-Aged Rats," (in eng), *Endocrinology,* vol. 158, no. 1, pp. 69-83, Jan 1 2017, doi: 10.1210/en.2016-1516.

[76] D. L. Lei *et al.*, "Effects of estrogen and raloxifene on neuroglia number and morphology in the hippocampus of aged female mice," (in eng), *Neuroscience,* vol. 121, no. 3, pp. 659-66, 2003, doi: 10.1016/s0306-4522(03)00245-8.
[77] V. Benedusi, C. Meda, S. Della Torre, G. Monteleone, E. Vegeto, and A. Maggi, "A lack of ovarian function increases neuroinflammation in aged mice," (in eng), *Endocrinology,* vol. 153, no. 6, pp. 2777-88, Jun 2012, doi: 10.1210/en.2011-1925.
[78] A. Prat *et al.*, "A novel mouse model of Alzheimer's disease with chronic estrogen deficiency leads to glial cell activation and hypertrophy," (in eng), *J Aging Res,* vol. 2011, p. 251517, 2011, doi: 10.4061/2011/251517.
[79] M. T. Heneka *et al.*, "Neuroinflammation in Alzheimer's disease," (in eng), *Lancet Neurol,* vol. 14, no. 4, pp. 388-405, Apr 2015, doi: 10.1016/s1474-4422(15)70016-5.
[80] P. Hemond, M. Migliore, G. A. Ascoli, and D. B. Jaffe, "The membrane response of hippocampal CA3b pyramidal neurons near rest: Heterogeneity of passive properties and the contribution of hyperpolarization-activated currents," *Neuroscience,* vol. 160, no. 2, pp. 359-70, May 5 2009, doi: 10.1016/j.neuroscience.2009.01.082.
[81] L. Wittner and R. Miles, "Factors defining a pacemaker region for synchrony in the hippocampus," *J Physiol,* vol. 584, no. Pt 3, pp. 867-83, Nov 1 2007, doi: 10.1113/jphysiol.2007.138131.
[82] M. S. Cembrowski, J. L. Bachman, L. Wang, K. Sugino, B. C. Shields, and N. Spruston, "Spatial Gene-Expression Gradients Underlie Prominent Heterogeneity of CA1 Pyramidal Neurons," *Neuron,* vol. 89, no. 2, pp. 351-68, Jan 20 2016, doi: 10.1016/j.neuron.2015.12.013.
[83] C. L. Thompson *et al.*, "Genomic anatomy of the hippocampus," *Neuron,* vol. 60, no. 6, pp. 1010-21, Dec 26 2008, doi: 10.1016/j.neuron.2008.12.008.
[84] K. Wu, K. J. Canning, and L. S. Leung, "Functional interconnections between CA3 and the dentate gyrus revealed by current source density analysis," *Hippocampus,* vol. 8, no. 3, pp. 217-30, 1998, doi: 10.1002/(SICI)1098-1063(1998)8:3<217::AID-HIPO5>3.0.CO;2-G.
[85] Q. Sun, A. Sotayo, A. S. Cazzulino, A. M. Snyder, C. A. Denny, and S. A. Siegelbaum, "Proximodistal Heterogeneity of Hippocampal CA3 Pyramidal Neuron Intrinsic Properties, Connectivity, and Reactivation during Memory Recall," *Neuron,* vol. 95, no. 3, pp. 656-672 e3, Aug 2 2017, doi: 10.1016/j.neuron.2017.07.012.
[86] G. Yakemow *et al.*, "Investigating neural markers of Alzheimer's disease in posttraumatic stress disorder using machine learning algorithms and magnetic resonance imaging," *Front Neurol,* vol. 15, p. 1470727, 2024, doi: 10.3389/fneur.2024.1470727.
[87] T. A. Van Kempen *et al.*, "Sex and estrogen receptor expression influence opioid peptide levels in the mouse hippocampal mossy fiber pathway," *Neuroscience letters,* vol. 552, pp. 66-70, Sep 27 2013, doi: 10.1016/j.neulet.2013.07.048.
[88] K. L. Mitterling *et al.*, "Cellular and subcellular localization of estrogen and progestin receptor immunoreactivities in the mouse hippocampus," (in eng), *J Comp Neurol,* vol. 518, no. 14, pp. 2729-43, Jul 15 2010, doi: 10.1002/cne.22361.
[89] I. Azcoitia, A. Sierra, and L. M. Garcia-Segura, "Localization of estrogen receptor beta-immunoreactivity in astrocytes of the adult rat brain," (in eng), *Glia,* vol. 26, no. 3, pp. 260-7, May 1999.
[90] S. Sakuma, D. Tokuhara, H. Hattori, O. Matsuoka, and T. Yamano, "Expression of estrogen receptor alpha and beta in reactive astrocytes at the male rat hippocampus after status epilepticus," (in eng), *Neuropathology,* vol. 29, no. 1, pp. 55-62, Feb 2009, doi: 10.1111/j.1440-1789.2008.00946.x.
[91] E. M. Waters *et al.*, "G-protein-coupled estrogen receptor 1 is anatomically positioned to modulate synaptic plasticity in the mouse hippocampus," (in eng), *J Neurosci,* vol. 35, no. 6, pp. 2384-97, Feb 11 2015, doi: 10.1523/jneurosci.1298-14.2015.

[92] G. M. Rune, U. Wehrenberg, J. Prange-Kiel, L. Zhou, G. Adelmann, and M. Frotscher, "Estrogen up-regulates estrogen receptor alpha and synaptophysin in slice cultures of rat hippocampus," (in eng), *Neuroscience,* vol. 113, no. 1, pp. 167-75, 2002, doi: 10.1016/s0306-4522(02)00152-5.
[93] M. M. Adams *et al.*, "Estrogen and aging affect the subcellular distribution of estrogen receptor-alpha in the hippocampus of female rats," (in eng), *J Neurosci,* vol. 22, no. 9, pp. 3608-14, May 1 2002, doi: 10.1523/jneurosci.22-09-03608.2002.
[94] D. J. Stone, Y. Song, C. P. Anderson, K. K. Krohn, C. E. Finch, and I. Rozovsky, "Bidirectional transcription regulation of glial fibrillary acidic protein by estradiol in vivo and in vitro," (in eng), *Endocrinology,* vol. 139, no. 7, pp. 3202-9, Jul 1998, doi: 10.1210/endo.139.7.6084.
[95] Y. L. Ma *et al.*, "Estrogen regulates the expression of Ndrg2 in astrocytes," (in eng), *Brain Res,* vol. 1569, pp. 1-8, Jun 20 2014, doi: 10.1016/j.brainres.2014.04.036.
[96] D. A. Cinalli, Jr., S. J. Cohen, M. Calubag, G. Oz, L. Zhou, and R. W. Stackman, Jr., "DREADD-inactivation of dorsal CA1 pyramidal neurons in mice impairs retrieval of object and spatial memories," (in eng), *Hippocampus,* vol. 33, no. 1, pp. 6-17, Jan 2023, doi: 10.1002/hipo.23484.
[97] Y. Ma *et al.*, "Estrogen replacement therapy-induced neuroprotection against brain ischemia-reperfusion injury involves the activation of astrocytes via estrogen receptor β," (in eng), *Sci Rep,* vol. 6, p. 21467, Feb 19 2016, doi: 10.1038/srep21467.
[98] A. Bosson, A. Paumier, S. Boisseau, M. Jacquier-Sarlin, A. Buisson, and M. Albrieux, "TRPA1 channels promote astrocytic Ca(2+) hyperactivity and synaptic dysfunction mediated by oligomeric forms of amyloid-β peptide," (in eng), *Mol Neurodegener,* vol. 12, no. 1, p. 53, Jul 6 2017, doi: 10.1186/s13024-017-0194-8.
[99] Q. Dong, J. Kim, L. Nguyen, Q. Bu, and Q. Chang, "An Astrocytic Influence on Impaired Tonic Inhibition in Hippocampal CA1 Pyramidal Neurons in a Mouse Model of Rett Syndrome," (in eng), *J Neurosci,* vol. 40, no. 32, pp. 6250-6261, Aug 5 2020, doi: 10.1523/jneurosci.3042-19.2020.
[100] Z. Šišková *et al.*, "Dendritic structural degeneration is functionally linked to cellular hyperexcitability in a mouse model of Alzheimer's disease," (in eng), *Neuron,* vol. 84, no. 5, pp. 1023-33, Dec 3 2014, doi: 10.1016/j.neuron.2014.10.024.
[101] K. D. Phelan, U. T. Shwe, H. Wu, and F. Zheng, "Investigating Contributions of Canonical Transient Receptor Potential Channel 3 to Hippocampal Hyperexcitability and Seizure-Induced Neuronal Cell Death," (in eng), *Int J Mol Sci,* vol. 25, no. 11, Jun 6 2024, doi: 10.3390/ijms25116260.
[102] Z. Lei, P. Deng, J. Li, and Z. C. Xu, "Alterations of A-type potassium channels in hippocampal neurons after traumatic brain injury," (in eng), *J Neurotrauma,* vol. 29, no. 2, pp. 235-45, Jan 20 2012, doi: 10.1089/neu.2010.1537.
[103] C. D. Courtney *et al.*, "Optoα1AR activation in astrocytes modulates basal hippocampal synaptic excitation and inhibition in a stimulation-specific manner," (in eng), *Hippocampus,* vol. 33, no. 12, pp. 1277-1291, Dec 2023, doi: 10.1002/hipo.23580.
[104] K. Bohmbach *et al.*, "An astrocytic signaling loop for frequency-dependent control of dendritic integration and spatial learning," (in eng), *Nat Commun,* vol. 13, no. 1, p. 7932, Dec 24 2022, doi: 10.1038/s41467-022-35620-8.
[105] Y. Wang *et al.*, "Astrocyte-secreted IL-33 mediates homeostatic synaptic plasticity in the adult hippocampus," (in eng), *Proc Natl Acad Sci U S A,* vol. 118, no. 1, Jan 5 2021, doi: 10.1073/pnas.2020810118.
[106] P. I. Ortinski *et al.*, "Selective induction of astrocytic gliosis generates deficits in neuronal inhibition," (in eng), *Nat Neurosci,* vol. 13, no. 5, pp. 584-91, May 2010, doi: 10.1038/nn.2535.

[107] L. Park, J. Anrather, C. Forster, K. Kazama, G. A. Carlson, and C. Iadecola, "Abeta-induced vascular oxidative stress and attenuation of functional hyperemia in mouse somatosensory cortex," (in eng), *J Cereb Blood Flow Metab,* vol. 24, no. 3, pp. 334-42, Mar 2004, doi: 10.1097/01.wcb.0000105800.49957.1e.
[108] K. Niwa, K. Kazama, L. Younkin, S. G. Younkin, G. A. Carlson, and C. Iadecola, "Cerebrovascular autoregulation is profoundly impaired in mice overexpressing amyloid precursor protein," (in eng), *Am J Physiol Heart Circ Physiol,* vol. 283, no. 1, pp. H315-23, Jul 2002, doi: 10.1152/ajpheart.00022.2002.
[109] M. Tolar, J. Hey, A. Power, and S. Abushakra, "Neurotoxic Soluble Amyloid Oligomers Drive Alzheimer's Pathogenesis and Represent a Clinically Validated Target for Slowing Disease Progression," (in eng), *Int J Mol Sci,* vol. 22, no. 12, Jun 14 2021, doi: 10.3390/ijms22126355.
[110] M. Habashi *et al.*, "Early diagnosis and treatment of Alzheimer's disease by targeting toxic soluble Aβ oligomers," (in eng), *Proc Natl Acad Sci U S A,* vol. 119, no. 49, p. e2210766119, Dec 6 2022, doi: 10.1073/pnas.2210766119.
[111] V. Matafora *et al.*, "Proteomics of the astrocyte secretome reveals changes in their response to soluble oligomeric Aβ," (in eng), *J Neurochem,* vol. 166, no. 2, pp. 346-366, Jul 2023, doi: 10.1111/jnc.15875.
[112] M. K. Tong, A. Thakur, T. Yang, S. K. Wong, W. K. Li, and Y. Lee, "Amyloid-β oligomer-induced neurotoxicity by exosomal interactions between neuron and microglia," (in eng), *Biochem Biophys Res Commun,* vol. 727, p. 150312, Oct 1 2024, doi: 10.1016/j.bbrc.2024.150312.
[113] F. Xu *et al.*, "Early-onset subicular microvascular amyloid and neuroinflammation correlate with behavioral deficits in vasculotropic mutant amyloid beta-protein precursor transgenic mice," (in eng), *Neuroscience,* vol. 146, no. 1, pp. 98-107, Apr 25 2007, doi: 10.1016/j.neuroscience.2007.01.043.
[114] M. Padurariu, A. Ciobica, I. Mavroudis, D. Fotiou, and S. Baloyannis, "Hippocampal neuronal loss in the CA1 and CA3 areas of Alzheimer's disease patients," (in eng), *Psychiatr Danub,* vol. 24, no. 2, pp. 152-8, Jun 2012.
[115] G. A. Kerchner, G. K. Deutsch, M. Zeineh, R. F. Dougherty, M. Saranathan, and B. K. Rutt, "Hippocampal CA1 apical neuropil atrophy and memory performance in Alzheimer's disease," (in eng), *Neuroimage,* vol. 63, no. 1, pp. 194-202, Oct 15 2012, doi: 10.1016/j.neuroimage.2012.06.048.
[116] T. M. Pirttimaki *et al.*, "α7 Nicotinic receptor-mediated astrocytic gliotransmitter release: Aβ effects in a preclinical Alzheimer's mouse model," (in eng), *PLoS One,* vol. 8, no. 11, p. e81828, 2013, doi: 10.1371/journal.pone.0081828.
[117] S. W. Mitra *et al.*, "Immunolocalization of estrogen receptor beta in the mouse brain: comparison with estrogen receptor alpha," (in eng), *Endocrinology,* vol. 144, no. 5, pp. 2055-67, May 2003, doi: 10.1210/en.2002-221069.
[118] N. G. Weiland, C. Orikasa, S. Hayashi, and B. S. McEwen, "Distribution and hormone regulation of estrogen receptor immunoreactive cells in the hippocampus of male and female rats," (in eng), *J Comp Neurol,* vol. 388, no. 4, pp. 603-12, Dec 1 1997, doi: 10.1002/(sici)1096-9861(19971201)388:4<603::aid-cne8>3.0.co;2-6.
[119] P. J. Shughrue and I. Merchenthaler, "Evidence for novel estrogen binding sites in the rat hippocampus," (in eng), *Neuroscience,* vol. 99, no. 4, pp. 605-12, 2000, doi: 10.1016/s0306-4522(00)00242-6.
[120] T. Tsurugizawa *et al.*, "Estrogen induces rapid decrease in dendritic thorns of CA3 pyramidal neurons in adult male rat hippocampus," (in eng), *Biochem Biophys Res Commun,* vol. 337, no. 4, pp. 1345-52, Dec 2 2005, doi: 10.1016/j.bbrc.2005.09.188.

[121] C. J. Pike, "Estrogen modulates neuronal Bcl-xL expression and beta-amyloid-induced apoptosis: relevance to Alzheimer's disease," (in eng), *J Neurochem,* vol. 72, no. 4, pp. 1552-63, Apr 1999, doi: 10.1046/j.1471-4159.1999.721552.x.

FIGURE LEGENDS

Figure 1: Timeline of experimental procedures. VCD (130 mg/kg, i.p.) was injected for 3 weeks, 5 days per week beginning at approximately postnatal day (PND) 58. The extracellular deposition of Aß plaques was expected to begin at ~PND 60, accompanied by microgliosis and astrogliosis. Behavioral assessments were performed for 2 weeks following the initiation of the peri-AOF phase. Brains were harvested at ~PND 130.

Figure 2: 4G8 labeling is differentially altered in select regions of the hippocampus of oil and peri-AOF female and male 5xFAD mice. (A,B) Low-magnification photomicrographs of 4G8 labeling in the rostral **(A)** and caudal **(B)** hippocampus. Boxes indicate regions of the CA1, CA3a, CA3b, dentate gyrus (DG), and subiculum (Sub) that were sampled. **(C,D,E)** Representative photomicrographs showing 4G8 labeling in the rostral CA1 of 5xFAD-oil **(C)**, 5xFAD-VCD **(D)**, and 5xFAD-male mice **(E)**. **(F)** In the rostral CA1 PCL, and dSR, 5xFAD-male mice show significantly less 4G8 labeling than 5xFAD-oil and 5xFAD-VCD female mice. In the rostral CA1 nSR, 5xFAD-male mice show significantly less 4G8 labeling than 5xFAD-oil female mice. **(G,H,I)** Representative photomicrographs showing 4G8 labeling in the CA3b of 5xFAD-oil **(G)**, 5xFAD-VCD **(H)**, and 5xFAD-male mice **(I)**. **(J)** In the CA3b PCL, 5xFAD-VCD female mice show greater 4G8 labeling than both 5xFAD-oil female and 5xFAD-male mice. In the CA3b SLu, 5xFAD-VCD female mice show greater 4G8 labeling than 5xFAD-male mice. * $p < 0.05$; ** $p < 0.01$ by One-way ANOVA with Tukey's post-hoc comparisons. Data are expressed as mean +/- SEM, n = 11 animals per experimental group. Scale bars (A,B) = 500 μm, (C,D,E,G,H,I) = 200 μm.

Figure 3: Increased GFAP labeling is associated with peri-AOF and/or 5xFAD genotype in select regions of the hippocampus. (A,B) Low-magnification photomicrographs of GFAP labeling in the rostral **(A)** and caudal **(B)** hippocampus. Boxes indicate regions of the CA1, CA3a, CA3b, dentate gyrus (DG), and subiculum (Sub) that were sampled. **(C,D,E,F,G,H)** Representative photomicrographs showing GFAP labeling in the rostral CA1 of WT-oil **(C),** WT-VCD **(D)**, WT-male **(E)**, 5xFAD-oil **(F)**, 5xFAD-VCD **(G)**, and 5xFAD-male mice **(H)**. **(I)** In the rostral CA1 SO, the density of GFAP was increased in 5xFAD mice compared to WT mice, irrespective of sex/AOF treatment. In the PCL, WT-VCD female mice show greater GFAP density than WT-male mice. In the SLM, 5xFAD-male mice show more GFAP labeling than WT-male mice. **(J,K,L,M,N,O)** Representative photomicrographs showing GFAP labeling in the caudal CA1 of WT-oil **(J)**, WT-VCD **(K)**, WT-male **(L)**, 5xFAD-oil **(M)**, 5xFAD-VCD **(N)**, and 5xFAD-male mice **(O)**. **(P)** In the caudal CA1 SO, the density of GFAP was increased in 5xFAD mice compared to WT mice, irrespective of sex/AOF treatment. In the PCL WT-oil female mice show less GFAP labeling than 5xFAD-oil and WT-VCD female mice. In the SR, 5xFAD-oil female mice show greater GFAP density than WT-oil female mice. In the SLM, both 5xFAD-oil female and 5xFAD-male mice had greater GFAP labeling than WT-oil and WT-male mice, respectively. In the Sub, the density of GFAP was increased in 5xFAD mice compared to WT mice, irrespective of sex/AOF treatment, and 5xFAD-oil female mice showed greater GFAP labeling than 5xFAD-male mice. * $p < 0.05$; ** $p < 0.01$; **** $p < 0.0001$ by two-way ANOVA with Tukey's hoc multiple comparison analysis. Data are expressed as mean +/- SEM, n = 11 mice per experimental group. Scale bars (A,B) = 500 μm, (C,D,E,F,G,H,J,K,L,M,N,O) = 200 μm.

Figure 4: Increased GFAP labeling is associated with peri-AOF and/or 5xFAD genotype in select regions of the hippocampus. (A,B,C,D,E,F) Representative photomicrographs showing GFAP labeling in the rostral DG of WT-oil **(A)**, WT-VCD **(B)**, WT-male **(C)**, 5xFAD-oil **(D)**, 5xFAD-VCD **(E)**, and 5xFAD-male mice **(F)**. **(G)** In the rostral DG crest, 5xFAD-VCD female mice show increased GFAP labeling compared to WT-VCD female mice. In the hilus, 5xFAD-VCD female

and 5xFAD-male mice show more GFAP labeling than WT-VCD female and WT-male mice, respectively. **(H,I,J,K,L,M**) Representative photomicrographs showing GFAP labeling in the caudal DG of WT-oil **(H)**, WT-VCD **(I)**, WT-male **(J)**, 5xFAD-oil **(K)**, 5xFAD-VCD **(L)**, and 5xFAD-male mice **(M)**. **(N)** In the caudal DG crest, hilus, and db, the density of GFAP was increased in 5xFAD-male mice compared to WT-male mice. In the db, GFAP density was also higher in 5xFAD-oil female mice compared to WT-oil female mice. * $p < 0.05$; ** $p < 0.01$ by two-way ANOVA with Tukey's post hoc multiple comparison analysis. Data are expressed as mean +/- SEM, n = 11 animals per experimental group. Scale bar = 200 μm.

Figure 5: Increased Iba1 labeling is associated with peri-AOF and/or 5xFAD genotype in select regions of the hippocampus. (A,B) Low-magnification photomicrographs of Iba1 labeling in the rostral **(A)** and caudal **(B)** hippocampus. Boxes indicate regions of the CA1, CA3a, CA3b, dentate gyrus (DG), and subiculum (Sub) that were sampled. **(C,D,E,F,G,H)** Representative photomicrographs showing Iba1 labeling in the rostral CA1 of WT-oil **(C)**, WT-VCD (D), WT-male **(E)**, 5xFAD-oil **(F)**, 5xFAD-VCD **(G)**, and 5xFAD-male mice **(H)**. **(I)** In the rostral CA1 SO and PCL, the density of Iba1 was increased in 5xFAD-VCD female and 5xFAD-male mice compared to WT-VCD female and WT-male mice, respectively. In the PCL, Iba1 density was greater in 5xFAD-VCD female mice than 5xFAD-oil female mice. In the SLM, 5xFAD-male mice had more Iba1 labeling than WT-male mice. **(J,K,L,M,N,O)** Representative photomicrographs showing Iba1 labeling in the caudal CA1 of WT-oil **(J)**, WT-VCD **(K)**, WT-male **(L)**, 5xFAD-oil **(M)**, 5xFAD-VCD **(N)**, and 5xFAD-male mice **(O)**. **(P)** In the caudal CA1 SO, 5xFAD-VCD female and 5xFAD-male mice had increased Iba1 density compared to WT-VCD and WT-male mice, respectively. In the PCL, the density of Iba1 was increased in 5xFAD mice compared to WT mice irrespective of sex/AOF treatment. 5xFAD-VCD female mice also showed greater Iba1 labeling than 5xFAD-male mice. In the SR and SLM, 5xFAD-male mice had more Iba1 labeling than WT-male mice. In the Sub, 5xFAD mice had increased Iba1 density compared to WT mice irrespective of sex/AOF treatment. * $p < 0.05$; ** $p < 0.01$; *** $p < 0.001$; **** $p < 0.0001$ by two-way ANOVA with Tukey's post hoc multiple comparison analysis. Data are expressed as mean +/- SEM, n = 11 animals per experimental group. Scale bars (A,B) = 500 μm, (C,D,E,F,G,H,J,K,L,M,N,O) = 200 μm.

Figure 6: Increased Iba1 labeling is associated with peri-AOF and/or 5xFAD genotype in select regions of the hippocampus. (A,B,C,D,E,F) Representative photomicrographs showing Iba1 labeling in the rostral DG of WT-oil **(A)**, WT-VCD **(B)**, WT-male **(C)**, 5xFAD-oil **(D)**, 5xFAD-VCD **(E)**, and 5xFAD-male mice **(F)**. **(G)** In the rostral DG crest and db, 5xFAD-VCD female and 5xFAD-male mice showed greater Iba1 labeling than WT-VCD and WT-male mice, respectively. In the hilus, the density of Iba1 labeling was increased in 5xFAD mice compared to WT mice, irrespective of sex/AOF treatment. 5xFAD-VCD female mice also showed greater Iba1 labeling than 5xFAD-male mice. **(H,I,J,K,L,M)** Representative photomicrographs showing GFAP labeling in the caudal DG of WT-oil **(H)**, WT-VCD **(I)**, WT-male **(J)**, 5xFAD-oil **(K)**, 5xFAD-VCD **(L)**, and 5xFAD-male mice **(M)**. **(N)** In the caudal DG crest, 5xFAD-male mice had greater Iba1 labeling than WT-male mice. In the hilus and db, the density of Iba1 was increased in 5xFAD mice compared to WT mice, irrespective of sex/AOF treatment. * $p < 0.05$; ** $p < 0.01$; *** $p < 0.001$; **** $p < 0.0001$ by two-way ANOVA with Tukey's post hoc multiple comparison analysis. Data are expressed as mean +/- SEM, n= 11 animals per experimental group. Scale bar = 200 μm.

Figure 7: Cognition is not impaired in the Y-maze but is in the novel object recognition test in 5xFAD compared to WT mice. (A,B) In the Y-maze test, there were no significant differences in arm alternation behavior **(A)** or in the number of arm entries **(B)** between 5xFAD and WT mice. **(C)** Spontaneous motor activity tended to be decreased in 5xFAD-male mice compared to 5xFAD-VCD female mice. **(D)** total object exploratory time was not changed across experimental groups. **(E)** No significant differences were observed between groups in the percentage time spent

exploring the novel object. **(F)** Significant increase in time spent with the novel object vs familiar object was observed for WT male and female (oil and VCD), as well as in 5xFAD male mice. This difference is lost in 5xFAD females. ^ $p = 0.06$; * $p < 0.05$; ** $p < 0.01$; **** $p < 0.0001$ by one-way ANOVA with Sidak's post hoc multiple comparison analysis. Data are expressed as mean +/- SEM, n= 11 animals per experimental group.

Figure 8: Cognitive performance is differentially affected on the Barnes maze test in peri-AOF female mice. (A,B,C,D) There were no observed differences in motor activity (A,B) and learning performance (C,D) in 5xFAD mice compared to WT mice over time by 2way ANOVA. **(E,F)** WT-VCD female mice demonstrated memory deficits compared to WT-oil and 5xFAD-VCD female mice. * $p < 0.05$; ** $p < 0.01$ by 2way ANOVA with Tukey's post-hoc comparison analysis (A-D) or student's unpaired t-test (E,F). Data are expressed as mean +/- SEM, *N* = 11 animals per experimental group.

Suppl. Figure 1: 4G8 labeling is not altered in select regions of the hippocampus of across WT and 5xFAD experimental groups. (A-C). Representative photomicrographs showing 4G8 labeling in the caudal CA1 of 5xFAD-oil **(A)**, 5xFAD-VCD **(B)**, and 5xFAD-male mice **(C)**. (**D)** In the caudal CA1, there were no significant differences in 4G8 labeling between 5xFAD-oil, 5xFAD-VCD female, and 5xFAD-male mice. **(E-G)** Representative photomicrographs showing 4G8 labeling in the rostral CA3a of 5xFAD-oil **(E)**, 5xFAD-VCD **(F)**, and 5xFAD-male mice **(G)**. (**H)** In the CA3a, there were no significant differences in 4G8 labeling observed between 5xFAD-oil, 5xFAD-VCD female, and 5xFAD-male mice. (**I-K)** Representative photomicrographs showing 4G8 labeling in the rostral DG of 5xFAD-oil **(I)**, 5xFAD-VCD **(J)**, and 5xFAD-male mice **(K)**. **L.** In the rostral DG, there were no significant differences in 4G8 labeling observed between 5xFAD-oil, 5xFAD-VCD female, 5xFAD-male mice. (**M-O)** Representative photomicrographs showing 4G8 labeling in the caudal DG of 5xFAD-oil **(M)**, 5xFAD-VCD **(N)**, and 5xFAD-male mice **(O)**. (**P)** In the caudal DG, there were no significant differences in 4G8 labeling between 5xFAD-oil, 5xFAD-VCD female, and 5xFAD-male mice. Statistics was calculated by One-way ANOVA with Tukey's post-hoc multi comparison analysis. Data are expressed as mean +/- SEM, n= 11 mice/group. Scale bar = 200 μm.

Suppl. Figure 2: GFAP and Iba1 labeling is unchanged in the CA3a and CA3b regions of the hippocampus of WT and 5xFAD female and male mice. (A,B,C,D,E,F) Representative photomicrographs showing GFAP labeling in the rostral CA3a of WT-oil **(A)**, WT-VCD **(B)**, WT-male **(C)**, 5xFAD-oil **(D)**, 5xFAD-VCD **(E)**, and 5xFAD-male mice **(F)**. (**G)** In the CA3a, there were no significant differences in GFAP labeling across groups. **H,I,J,K,L,M.** Representative photomicrographs showing GFAP labeling in the rostral DG of WT-oil **(H)**, WT-VCD **(I)**, WT-male **(J)**, 5xFAD-oil **(K)**, 5xFAD-VCD **(L)**, and 5xFAD-male mice **(M)**. **N.** In the CA3b, there were no significant differences in GFAP labeling across groups. (**O,P,Q,R,S,T)** Representative photomicrographs showing Iba1 labeling in the rostral DG of WT-oil **(O)**, WT-VCD **(P)**, WT-male **(Q)**, 5xFAD-oil **(R)**, 5xFAD-VCD **(S)**, and 5xFAD-male mice **(T)**. (**U)** In the CA3a, there were no significant differences in Iba1 labeling across groups. (**V,W,X,Y,Z,AA).** Representative photomicrographs showing Iba1 labeling in the rostral DG of WT-oil **(V)**, WT-VCD **(W)**, WT-male **(X)**, 5xFAD-oil **(Y)**, 5xFAD-VCD **(Z)**, and 5xFAD-male mice **(AA)**. (**AB)** In the CA3a, there were no significant differences in Iba1 labeling across groups. Statistics was calculated by two-way ANOVA with Tukey's post hoc multiple comparison analysis. Data are expressed as mean +/- SEM, *n* = 11 animals per experimental group. Scale bar = 200 μm.

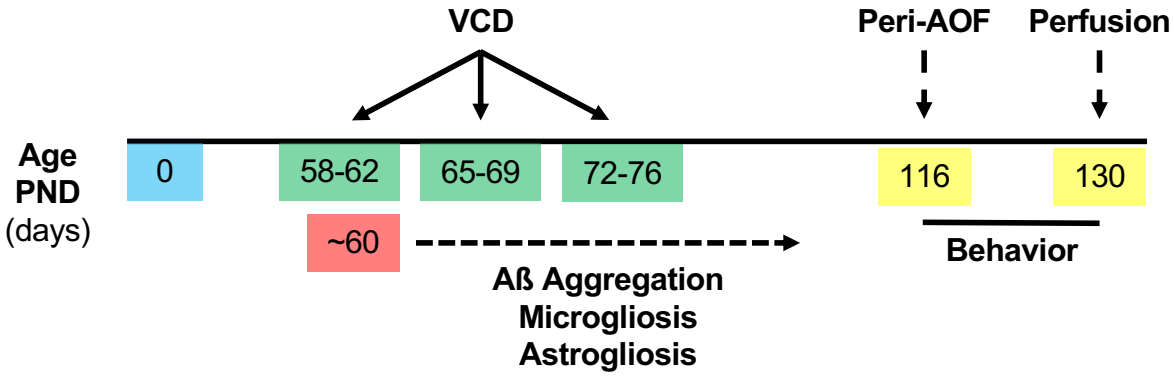
VCD
Peri-AOF
Perfusion
Age
PND
(days)
0
58-62
65-69
72-76
116
130
~60
Behavior
Aß Aggregation
Microgliosis
Astrogliosis

Fig. 1

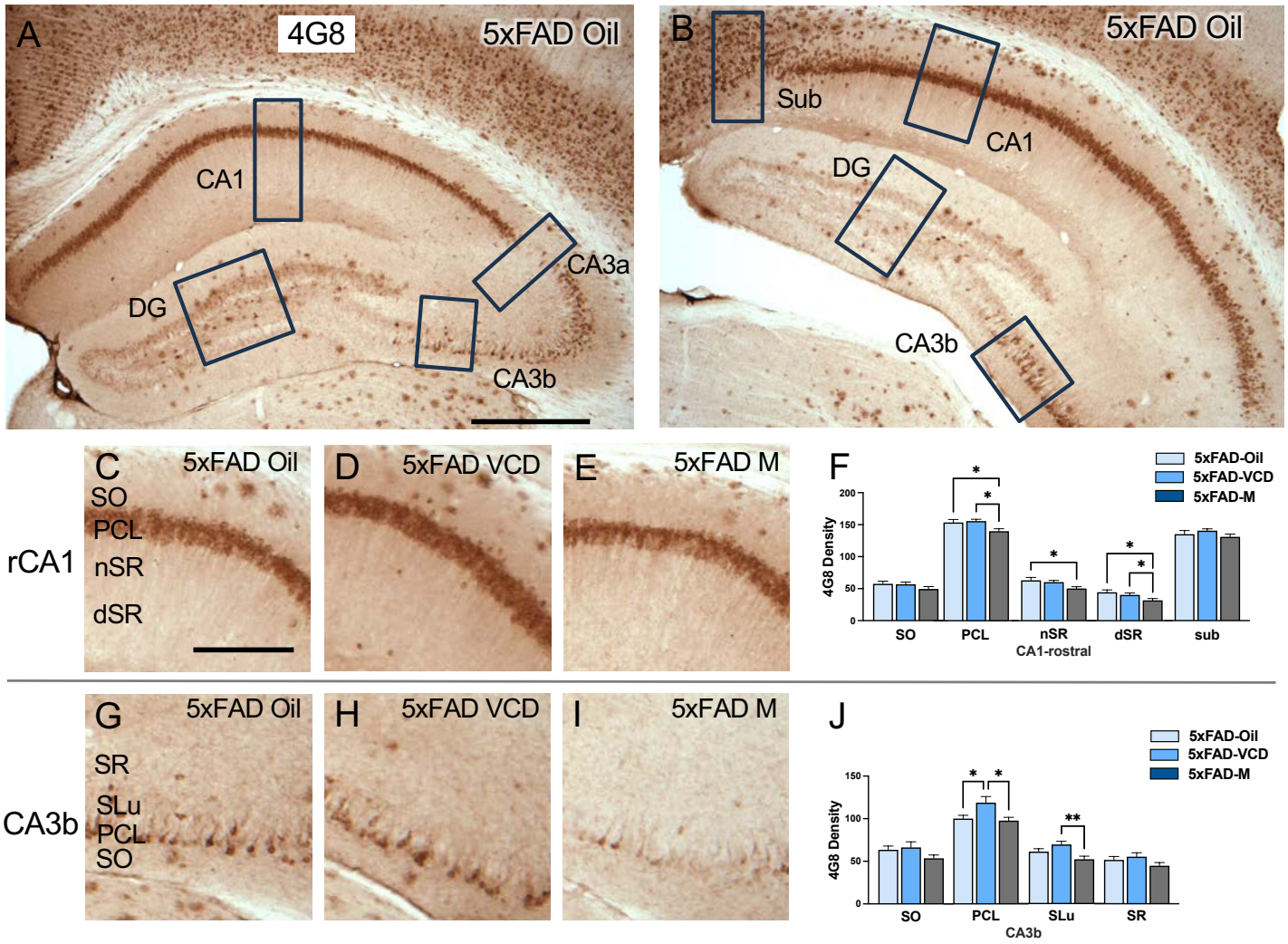
A
4G8
5xFAD Oil
CA1
DG
CA3a
CA3b
B
5xFAD Oil
Sub
CA1
DG
CA3b
C
5xFAD Oil
SO
PCL
nSR
dSR
rCA1
D
5xFAD VCD
E
5xFAD M
F
5xFAD-Oil
5xFAD-VCD
5xFAD-M
4G8 Density
SO
PCL
nSR
dSR
sub
CA1-rostral
G
5xFAD Oil
SR
SLu
PCL
SO
CA3b
H
5xFAD VCD
I
5xFAD M
J
5xFAD-Oil
5xFAD-VCD
5xFAD-M
4G8 Density
SO
PCL
SLu
SR
CA3b

Fig. 2

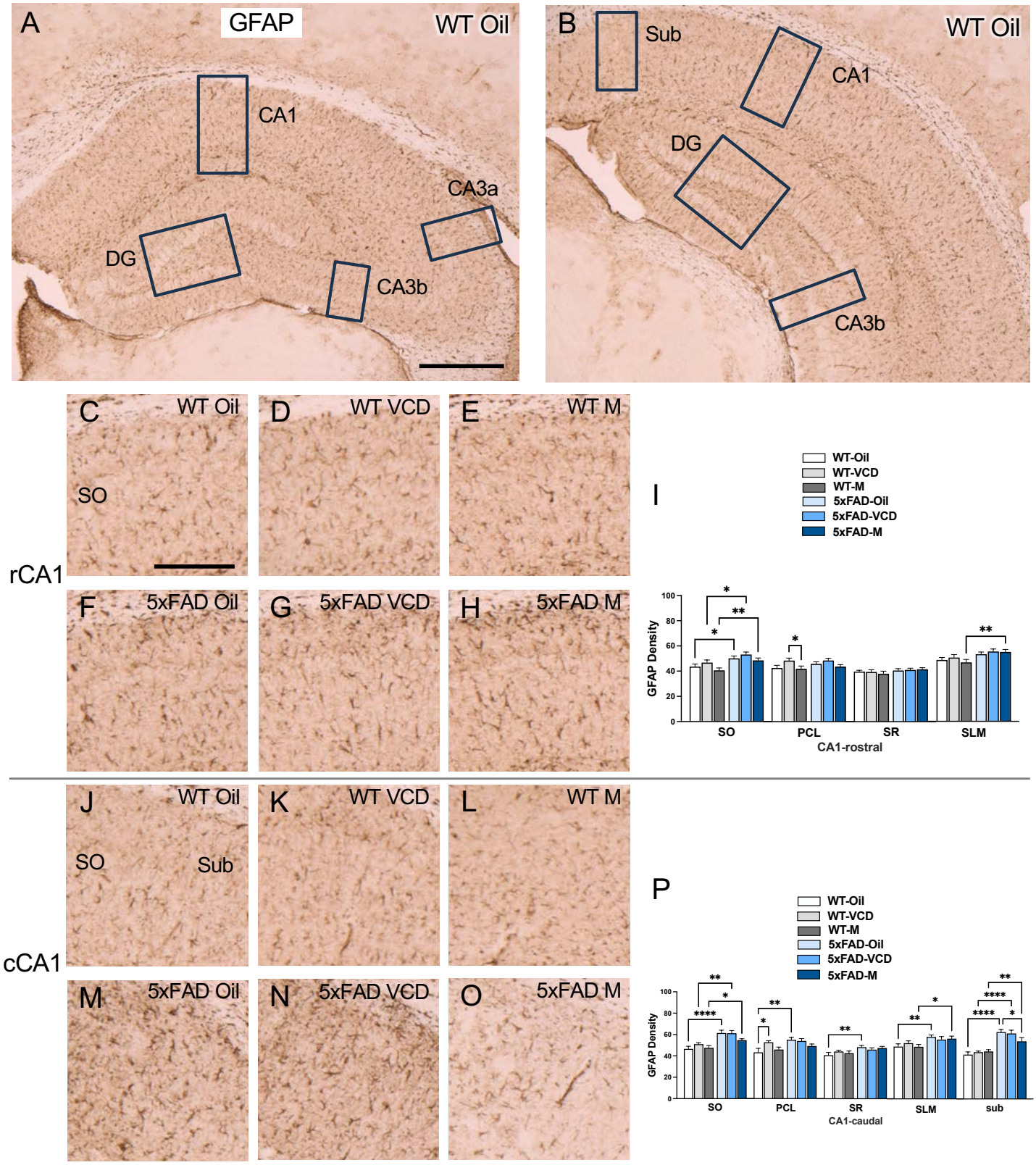
A
GFAP
WT Oil
CA1
CA3a
DG
CA3b
B
Sub
WT Oil
CA1
DG
CA3b
C
WT Oil
SO
D
WT VCD
E
WT M
rCA1
F
5xFAD Oil
G
5xFAD VCD
H
5xFAD M
I
WT-Oil
WT-VCD
WT-M
5xFAD-Oil
5xFAD-VCD
5xFAD-M
GFAP Density
SO
PCL
SR
SLM
CA1-rostral
J
WT Oil
SO
Sub
K
WT VCD
L
WT M
cCA1
M
5xFAD Oil
N
5xFAD VCD
O
5xFAD M
P
WT-Oil
WT-VCD
WT-M
5xFAD-Oil
5xFAD-VCD
5xFAD-M
GFAP Density
SO
PCL
SR
SLM
sub
CA1-caudal

Fig. 3

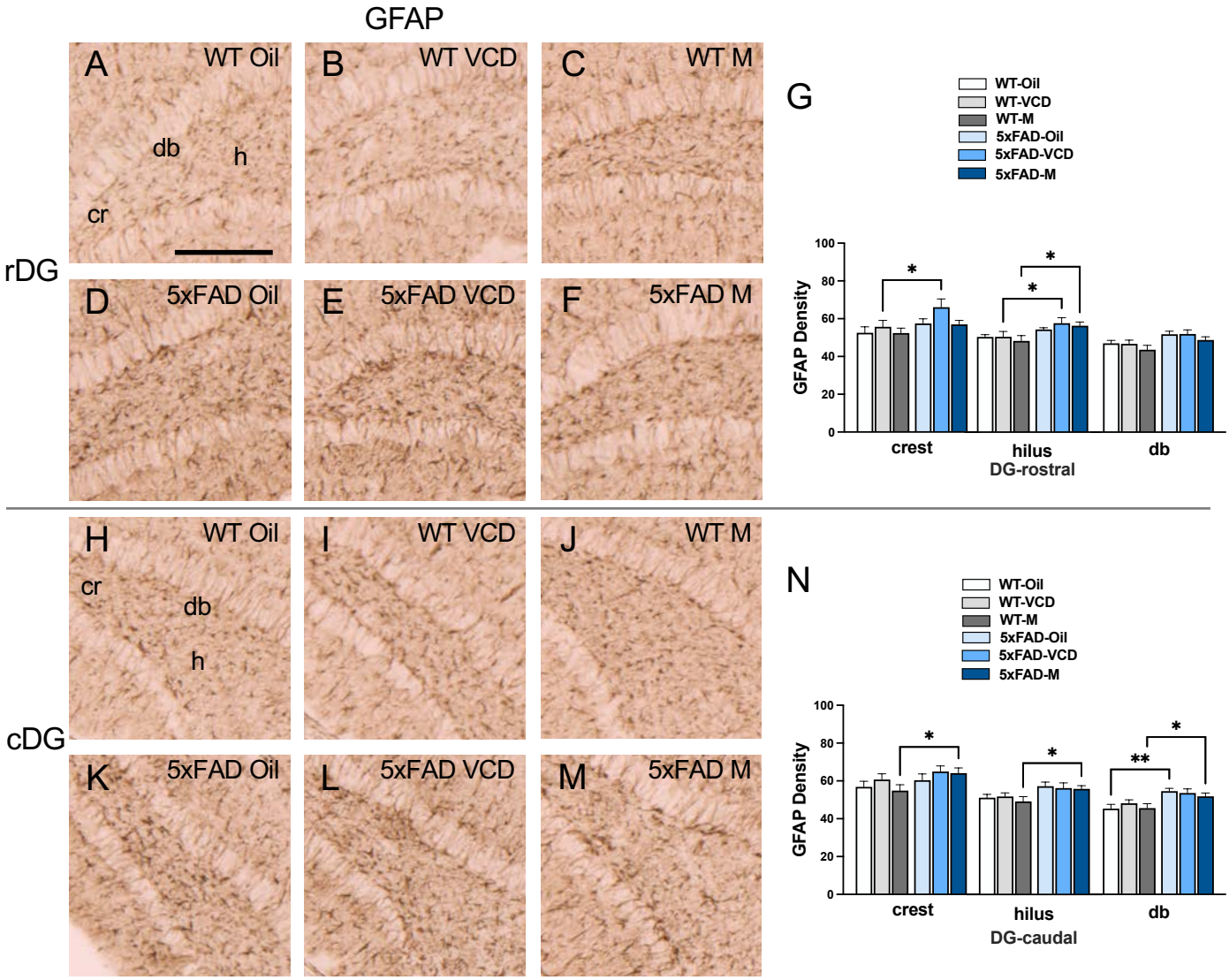
GFAP
A
WT Oil
db
h
cr
B
WT VCD
C
WT M
rDG
D
5xFAD Oil
E
5xFAD VCD
F
5xFAD M
G
WT-Oil
WT-VCD
WT-M
5xFAD-Oil
5xFAD-VCD
5xFAD-M
GFAP Density
100
80
60
40
20
0
*
*
*
crest
hilus
db
DG-rostral
H
WT Oil
cr
db
h
I
WT VCD
J
WT M
cDG
K
5xFAD Oil
L
5xFAD VCD
M
5xFAD M
N
WT-Oil
WT-VCD
WT-M
5xFAD-Oil
5xFAD-VCD
5xFAD-M
GFAP Density
100
80
60
40
20
0
*
*
**
*
crest
hilus
db
DG-caudal

Fig. 4

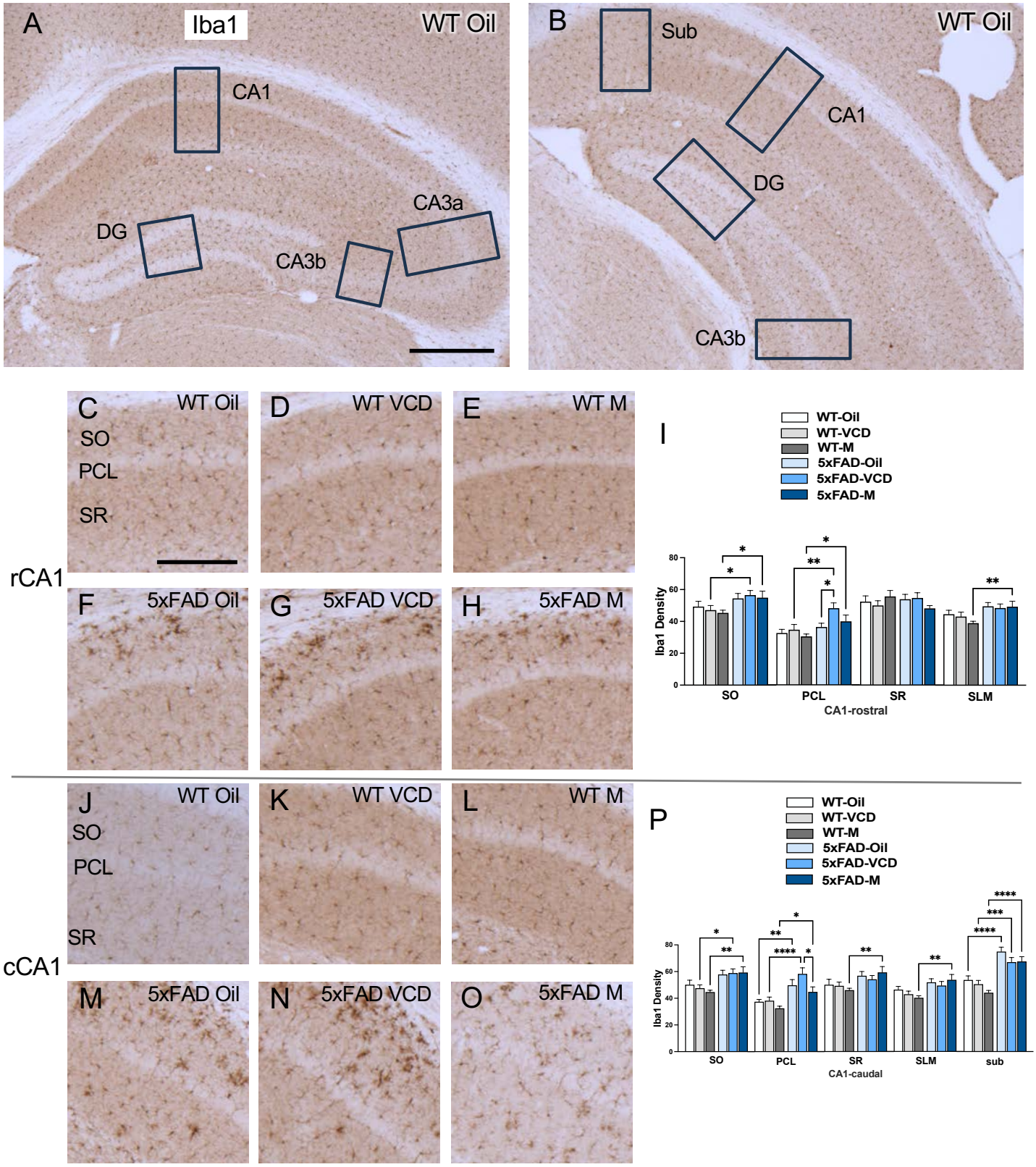
A
Iba1
WT Oil
CA1
DG
CA3a
CA3b
B
Sub
WT Oil
CA1
DG
CA3b
C
WT Oil
SO
PCL
SR
D
WT VCD
E
WT M
rCA1
F
5xFAD Oil
G
5xFAD VCD
H
5xFAD M
I
WT-Oil
WT-VCD
WT-M
5xFAD-Oil
5xFAD-VCD
5xFAD-M
Iba1 Density
SO
PCL
SR
SLM
CA1-rostral
J
WT Oil
SO
PCL
SR
K
WT VCD
L
WT M
cCA1
M
5xFAD Oil
N
5xFAD VCD
O
5xFAD M
P
WT-Oil
WT-VCD
WT-M
5xFAD-Oil
5xFAD-VCD
5xFAD-M
Iba1 Density
SO
PCL
SR
SLM
sub
CA1-caudal

Fig. 5

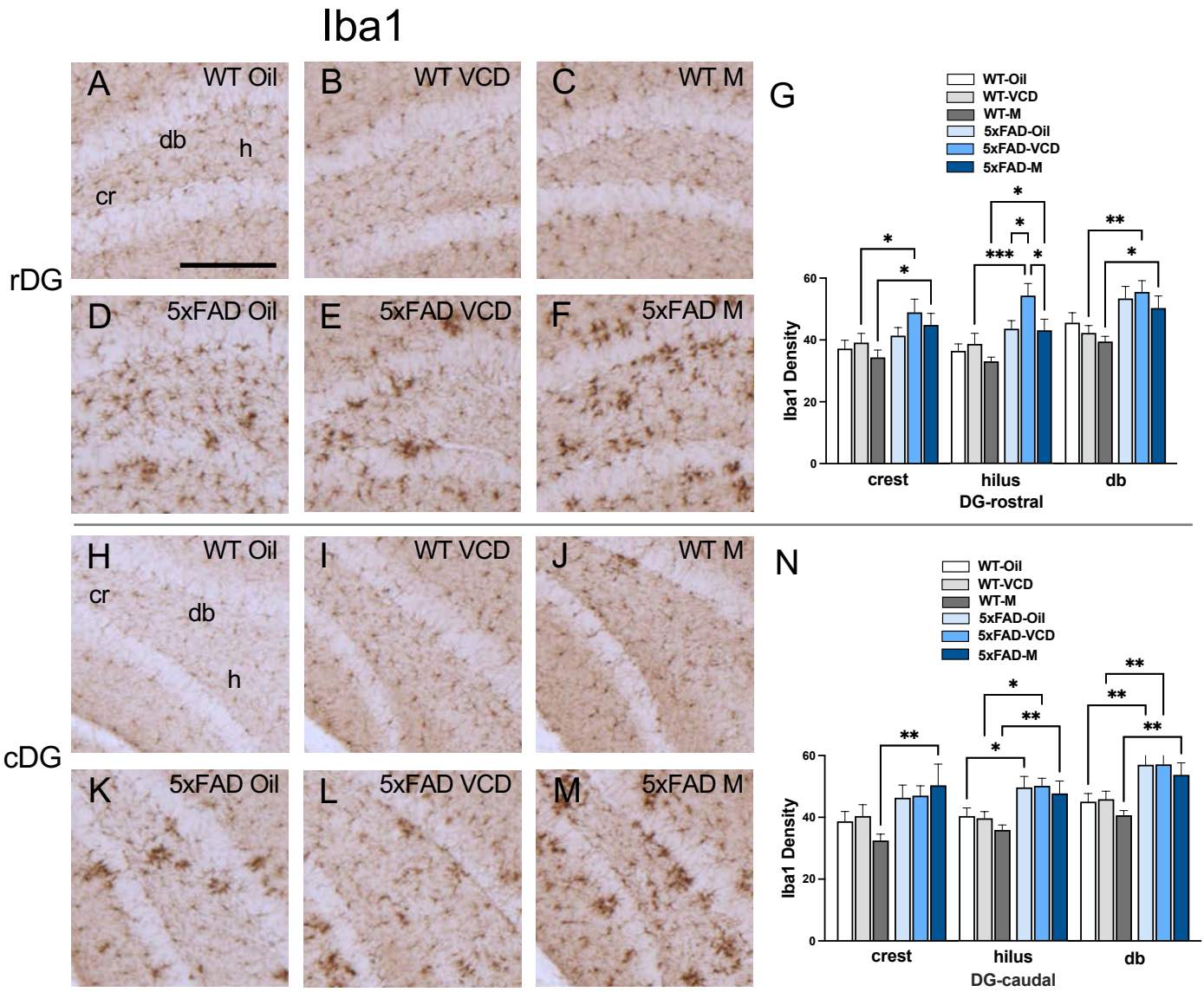
Iba1
A
WT Oil
db
h
cr
B
WT VCD
C
WT M
rDG
D
5xFAD Oil
E
5xFAD VCD
F
5xFAD M
G
WT-Oil
WT-VCD
WT-M
5xFAD-Oil
5xFAD-VCD
5xFAD-M
Iba1 Density
crest
hilus
db
DG-rostral
H
WT Oil
cr
db
h
I
WT VCD
J
WT M
cDG
K
5xFAD Oil
L
5xFAD VCD
M
5xFAD M
N
WT-Oil
WT-VCD
WT-M
5xFAD-Oil
5xFAD-VCD
5xFAD-M
Iba1 Density
crest
hilus
db
DG-caudal

Fig. 6

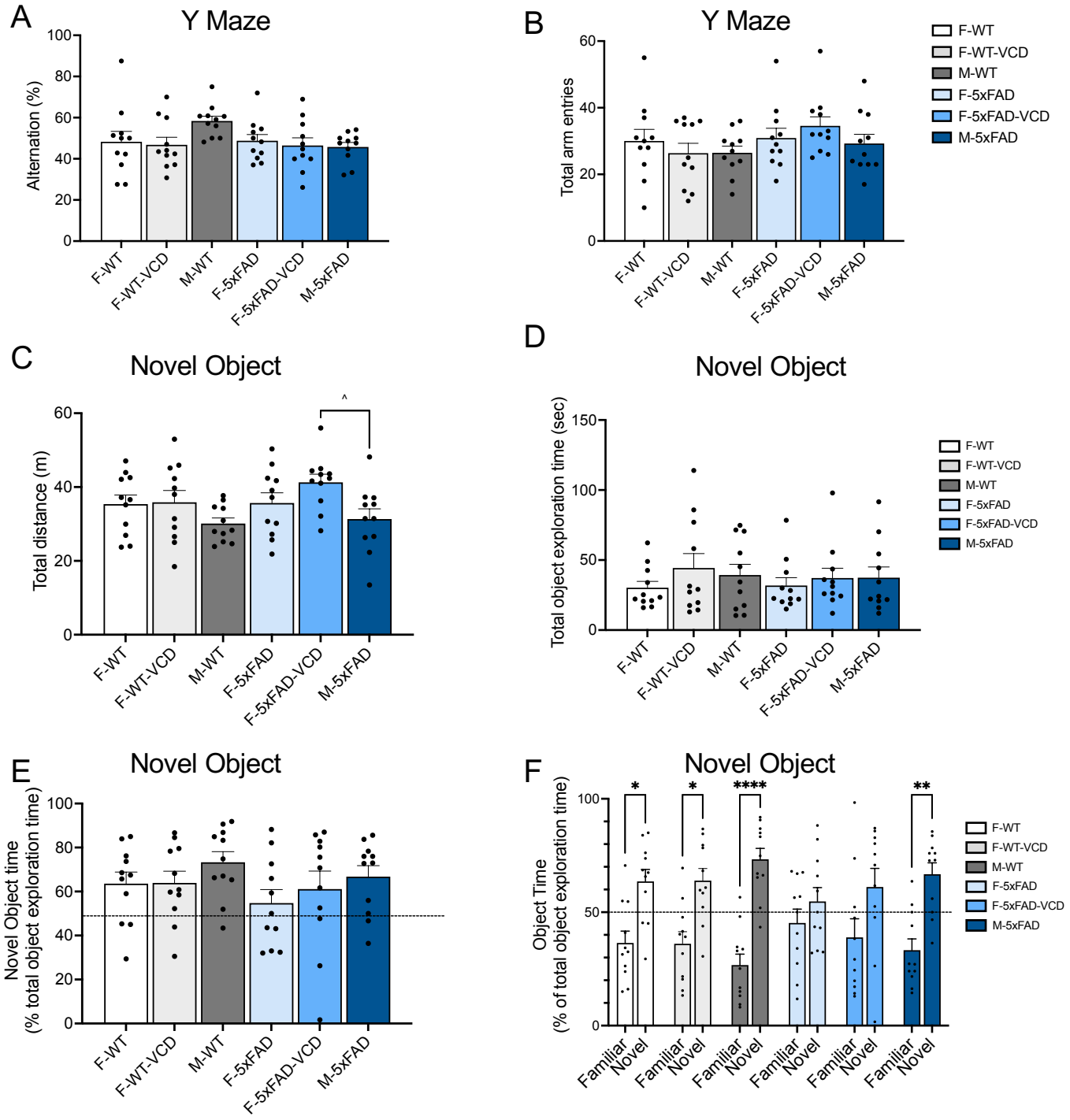
A
Y Maze
Alternation (%)
100
80
60
40
20
0
F-WT
F-WT-VCD
M-WT
F-5xFAD
F-5xFAD-VCD
M-5xFAD
B
Y Maze
Total arm entries
60
40
20
0
F-WT
F-WT-VCD
M-WT
F-5xFAD
F-5xFAD-VCD
M-5xFAD
C
Novel Object
Total distance (m)
60
40
20
0
^
D
Novel Object
Total object exploration time (sec)
150
100
50
0
E
Novel Object
Novel Object time
(% total object exploration time)
F
Novel Object
Object Time
(% of total object exploration time)
*
*
****
**
Familiar
Novel

Fig. 7

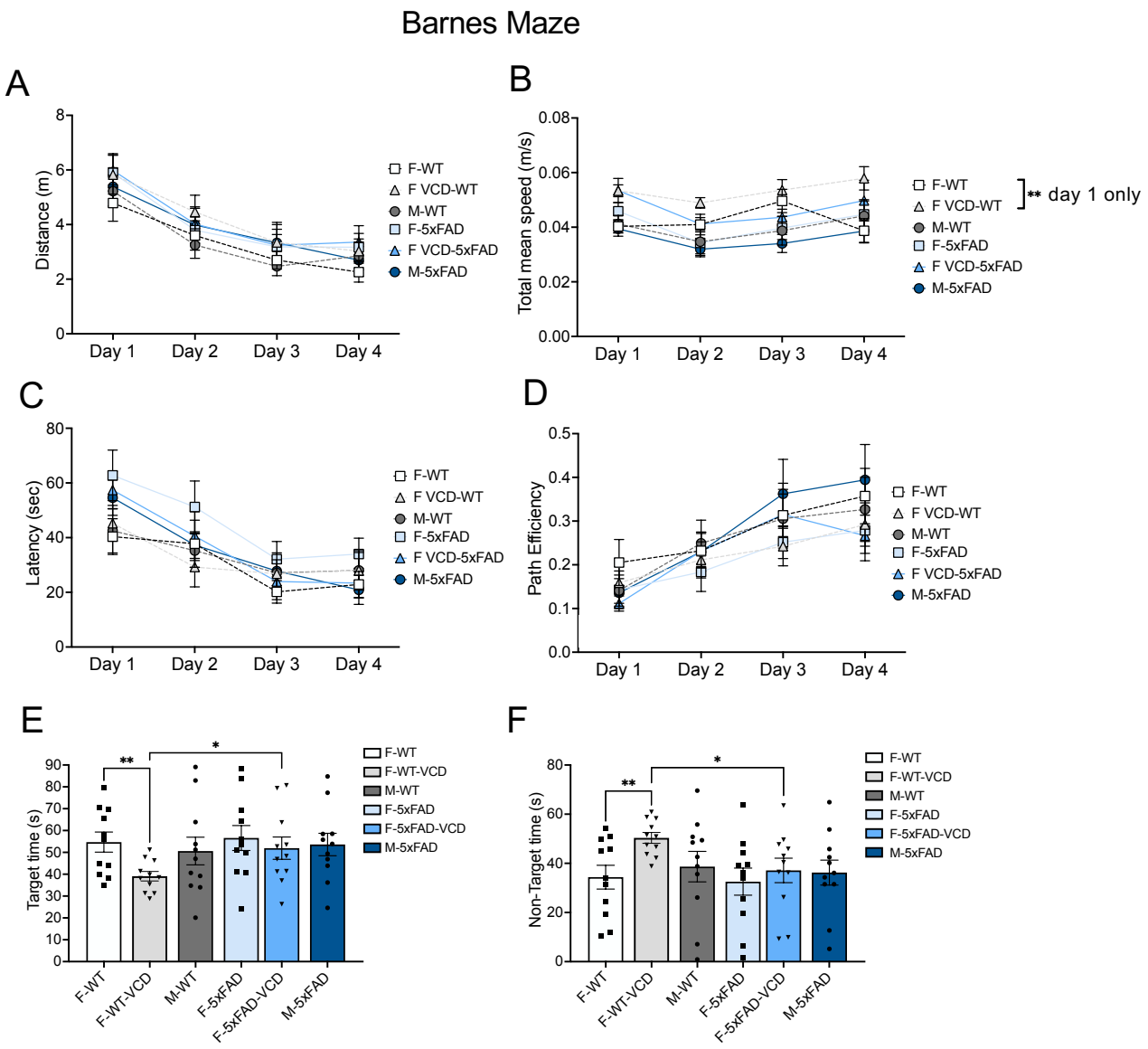
Barnes Maze
A
Distance (m)
Day 1
Day 2
Day 3
Day 4
F-WT
F VCD-WT
M-WT
F-5xFAD
F VCD-5xFAD
M-5xFAD
B
Total mean speed (m/s)
** day 1 only
C
Latency (sec)
D
Path Efficiency
E
Target time (s)
F-WT-VCD
F-5xFAD-VCD
F
Non-Target time (s)

Fig. 8

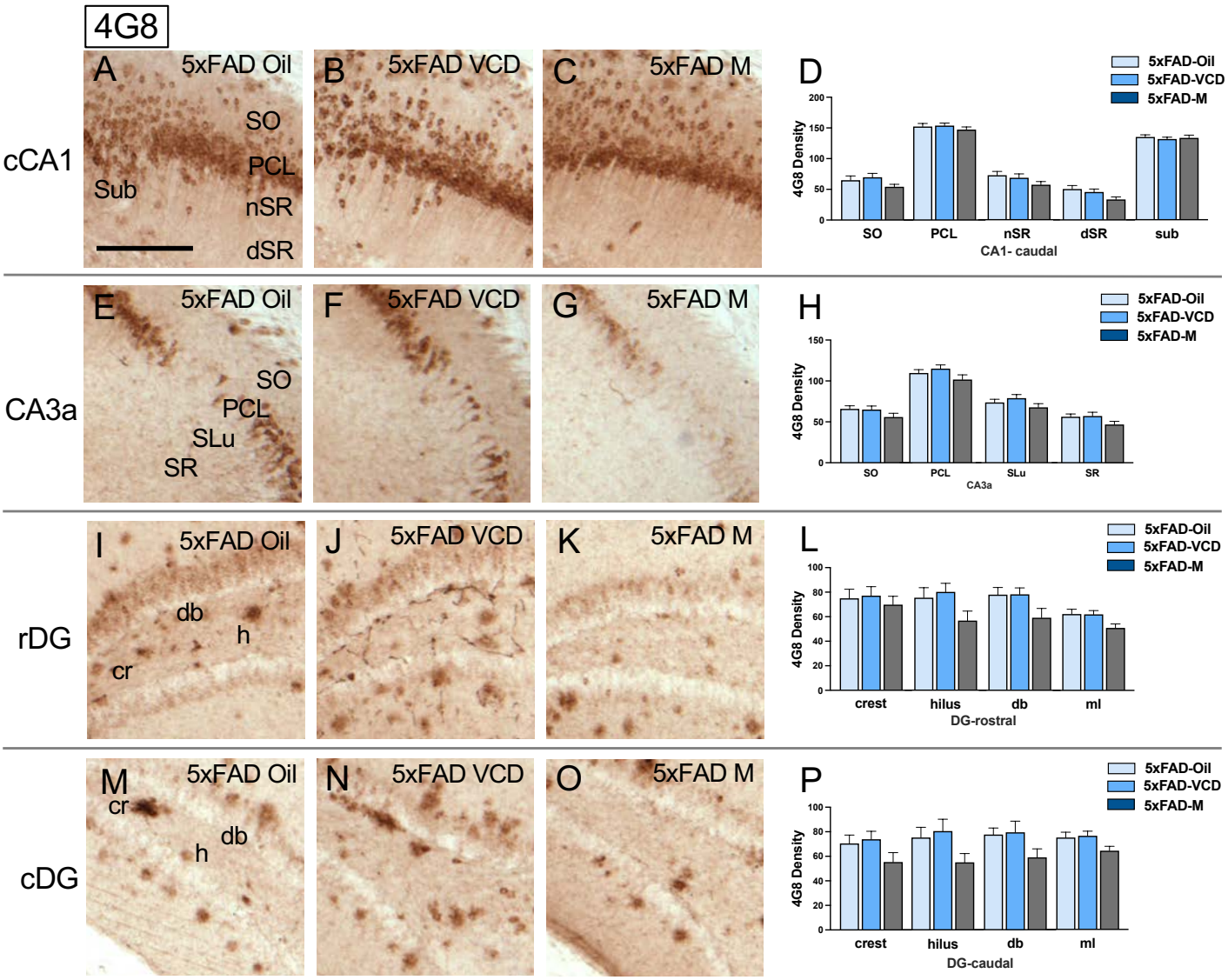
4G8
cCA1
A
5xFAD Oil
SO
PCL
Sub
nSR
dSR
B
5xFAD VCD
C
5xFAD M
D
5xFAD-Oil
5xFAD-VCD
5xFAD-M
4G8 Density
SO
PCL
nSR
dSR
sub
CA1- caudal
CA3a
E
5xFAD Oil
SO
PCL
SLu
SR
F
5xFAD VCD
G
5xFAD M
H
5xFAD-Oil
5xFAD-VCD
5xFAD-M
4G8 Density
SO
PCL
SLu
SR
CA3a
rDG
I
5xFAD Oil
db
h
cr
J
5xFAD VCD
K
5xFAD M
L
5xFAD-Oil
5xFAD-VCD
5xFAD-M
4G8 Density
crest
hilus
db
ml
DG-rostral
cDG
M
5xFAD Oil
cr
db
h
N
5xFAD VCD
O
5xFAD M
P
5xFAD-Oil
5xFAD-VCD
5xFAD-M
4G8 Density
crest
hilus
db
ml
DG-caudal

Suppl. Fig. 1

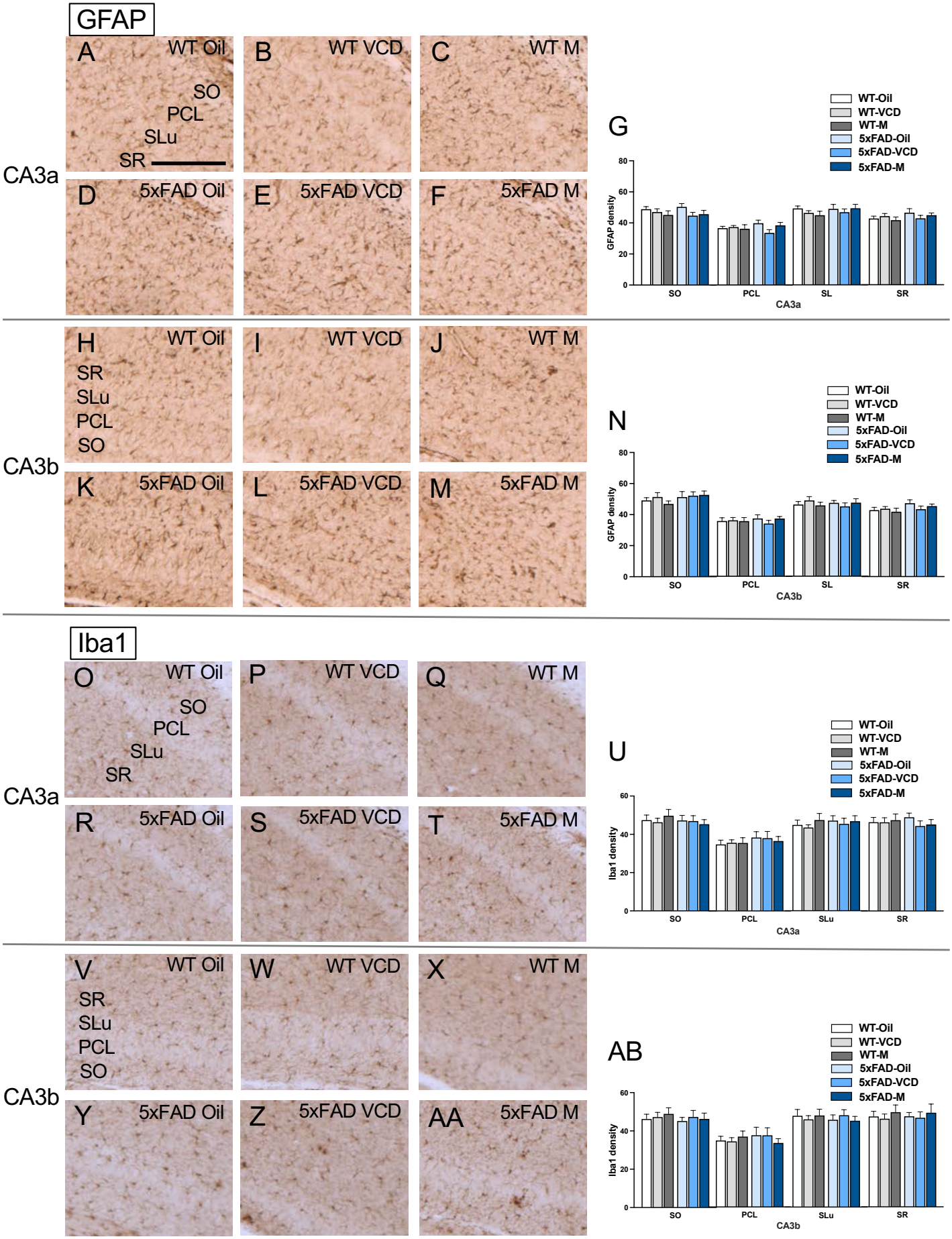
GFAP
A
WT Oil
SO
PCL
SLu
SR
B
WT VCD
C
WT M
CA3a
D
5xFAD Oil
E
5xFAD VCD
F
5xFAD M
G
WT-Oil
WT-VCD
WT-M
5xFAD-Oil
5xFAD-VCD
5xFAD-M
GFAP density
0
20
40
60
80
SO
PCL
SL
SR
CA3a
H
WT Oil
SR
SLu
PCL
SO
I
WT VCD
J
WT M
CA3b
K
5xFAD Oil
L
5xFAD VCD
M
5xFAD M
N
WT-Oil
WT-VCD
WT-M
5xFAD-Oil
5xFAD-VCD
5xFAD-M
GFAP density
0
20
40
60
80
SO
PCL
SL
SR
CA3b
Iba1
O
WT Oil
SO
PCL
SLu
SR
P
WT VCD
Q
WT M
CA3a
R
5xFAD Oil
S
5xFAD VCD
T
5xFAD M
U
WT-Oil
WT-VCD
WT-M
5xFAD-Oil
5xFAD-VCD
5xFAD-M
Iba1 density
0
20
40
60
SO
PCL
SLu
SR
CA3a
V
WT Oil
SR
SLu
PCL
SO
W
WT VCD
X
WT M
CA3b
Y
5xFAD Oil
Z
5xFAD VCD
AA
5xFAD M
AB
WT-Oil
WT-VCD
WT-M
5xFAD-Oil
5xFAD-VCD
5xFAD-M
Iba1 density
0
20
40
60
SO
PCL
SLu
SR
CA3b

Suppl. Fig. 2